FORCE MEASUREMENTS ON BLUFF CYLINDERS AND AEROELASTIC GALLOPING OF A RECTANGULAR CYLINDER

by

THOMAS V. SANTOSHAM

B.Sc. University of Strathclyde, Glasgow

A THESIS SUBMITTED IN PARTIAL FULFILLMENT OF THE

REQUIREMENTS FOR THE DEGREE OF

MASTER OF APPLIED SCIENCE

in the Department

of

Mechanical Engineering

We accept this thesis as conforming to the required standard

THE UNIVERSITY OF BRITISH COLUMBIA

JANUARY, 1966

In presenting this thesis in partial fulfilment of the requirements for an advanced degree at the University of British Columbia, I agree that the Library shall make it freely available for reference and study. I further agree that permission for extensive copying of this thesis for scholarly purposes may be granted by the Head of my Department or by his representatives. It is understood that copying or publication of this thesis for financial gain shall not be allowed without my written permission.

Department of Mechanical Engineering

The University of British Columbia
Vancouver 8, Canada

Date March 3 1966

ABSTRACT

Dynamic wind tunnel tests were made on plunging rectangular 2:1 and 1/2:1 cylinders and the results were compared with predictions of a quasi-steady theory. The velocity-amplitude and time-amplitude curves for those cylinders which oscillated were recorded. Dynamic tests were also performed on a 2:1 rectangular cylinder with a 10" splitter plate mounted on the wake centerline to prevent the vortex excitation. Direct static force measurements for the Reynolds number range $2 \times 10^4 < R_N < 7 \times 10^4$ were made for the rectangular 2:1 and 1/2:1 cylinders and the "D" section, using an Aerolab pyramidal strain gauge balance system. The quasi-steady theory used assumes that the instantaneous aerodynamic forces acting on the oscillating cylinder may be approximated by the static forces on the cylinder at an angle of attack equal to the apparent angle of attack of the oscillating cylinder at that instant. The above theory was also extended by including an expression for the vortex excitation.

The rectangular 2:1 cylinder for values of critical reduced wind speed U_o greater than 10 oscillated in agreement with the predictions of the quasi-steady approach. The rectangular 1/2:1 cylinder was found to be a "hard" oscillator as predicted by the quasi-steady theory. By the solution given by the quasi-steady theory the rectangular 2:1 cylinder which exhibits the galloping phenomenon in air flow will not gallop under similar conditions in water flow. In the Reynolds number range considered the static forces on the "D" Section were extremely Reynolds number dependent in the range of the angle of attack $36° \ll 60°$.

CONTENTS

Page No.

ILLUSTRATIONS

ACKNOWLEDGEMENTS

The author is indebted to Dr. G.V. Parkinson for his invaluable advice and supervision given throughout the whole research programme. The author also wishes to express appreciation to Mr. P. Hurren and J. Hoar, technicians, whose dedicated assistance on technical matters greatly accelerated the research programme.

Thanks must be expressed to the Mechanical Engineering Department for use of their facilities and to the Pharmacology Department for their help in designing the D.C. differential amplifier used in this investigation.

Financial assistance was received from the National Research Council of Canada, Grant A-586.

NOMENCLATURE

y = Lateral displacement of oscillating cylinder

h = Lateral dimension of cylinder section

b = Streamwise dimension of cylinder section

ℓ = Length of cylinder

m = Mass of oscillating system

r = Coefficient of viscous damping of oscillating system

k = Spring constant

$\omega = (k/m)^{1/2}$ = Circular frequency of free undamped oscillating system

V = Air velocity

V_{rel} = Air velocity relative to oscillating cylinder

α = Angle of attack of relative wind to cylinder section

$= \tan^{-1}(\dot{y}/V)$

ρ = Air density

p = Pressure

L = Aerodynamic lift on cylinder

D = Aerodynamic drag on cylinder

F_Y = Lateral aerodynamic force on cylinder

$$C_L = \frac{L}{(\rho/2)V^2_{rel}h\ell}$$

$$C_D = \frac{D}{(\rho/2)V^2_{rel}h\ell}$$

$$C_{Fy} = \frac{F_Y}{(\rho/2)V^2h\ell}$$

$U = V/(\omega h)$ = Dimensionless flow velocity

$Y = y/h$ = Dimensionless displacement

$\bar{Y}$ = Dimensionless oscillation amplitude

β = $r/(2m\omega)$ = Dimensionless damping coefficient

$n = \frac{\rho h^2 \ell}{2m}$ = Dimensionless mass parameter

$U_o = \frac{2\beta}{nA}$ = Critical air velocity

t = Time

$\tau = \omega t$ = Dimensionless time

$(\dot{})$ = Derivative with time

ν = Kinematic viscosity

$R_N = \frac{Vh}{\nu}$ = Reynolds Number

ω_1 = Fundamental circular Strouhal frequency

$S = fh/V = \frac{\omega_1 h}{2\pi V}$ = Strouhal number

$K_1 = \omega_1/\omega$

A.R. = b/h = Aspect ratio

A,B,C,D,E,F, = Coefficients of polynomial approximation to C_{Fy}

I. INTRODUCTION

This project was part of a continuing programme studying the aeroelastic instability of bluff cylinders. It is well known that bluff cylinders exhibit various forms of vibration when elastically mounted in a flow of air. Best known, perhaps, is the vortex-excited oscillation, in which the cylinder vibrates in a particular mode over a small discrete range of wind speeds containing that at which the fundamental frequency of the Karman Vortex street formed in the wake coincides with the natural frequency of the mode. Some cylinders, however, will begin to oscillate under conditions in which the frequency of vortex shedding is far removed from any elastic natural frequency of the cylinder. These bluff cylinders are termed aerodynamically unstable and exhibit galloping.

Some galloping instabilities require combined motion of the cylinder section in two or three degrees of freedom, the individual degrees of freedom being stable. Many of the observed cases of galloping, however, have been predominantly in one degree of freedom of the cylinder section, lateral translations in a horizontal wind normal to the cylinder axis. Because of its relative simplicity and importance, this form of galloping has been studied in this project.

In an earlier phase of the programme, Brooks[1] investigated the instability of bluff bodies of rectangular section and the 'D' section. He showed that for plunging oscillation the D-section and the short rectangles are stable at rest. The square section, however, did show strong instability. His thesis also contains a fairly complete historical background on the problem of aero-elastic instability of bluff

cylinders. Smith[2] with more sophisticated and accurate instrumentation extended Brooks' investigation of rectangular sections. His thesis also includes an extensive investigation into the unstable oscillation characteristics of the square section. Parkinson[3] showed that this oscillation can be analyzed as an aeroelastic non-linear oscillator using a quasi-steady theory; however, a similar investigation for the 2:1 rectangle did not show any agreement with Smith's experimental values.

The present investigation was undertaken to find the cause of such discrepancy. Extensive force measurements were also taken on the 1/2:1 rectangle and the "D" section. An attempt was made to find the experimental "hard" oscillation characteristics of the 1/2:1 rectangle, to check the theoretical value predicted by using the quasi-steady theory. Finally the effect of including the response function, due to the formation of wake vortices, on the differential equation given by the quasi-steady theory was investigated.

II. THEORY

2.1 Outline of Theory

A quasi-steady theory is used for predicting the model oscillation. This theory assumes that the instantaneous aerodynamic forces acting on the oscillating cylinder may be approximated by the forces on the stationary cylinder at an angle of attack equal to the apparent angle of attack of the oscillating cylinder at that instant. For a model with square cross-section, Parkinson and Smith[4] showed good agreement of experimental results with the quasi-steady theory. A simplified model of vortex excitation is also included in the following analysis.

The quasi-steady analysis without a vortex excitation term leads to a quasi-linear differential equation, of the autonomous type, of the form

$$\ddot{Y} + Y = \mu f(\dot{Y}) \qquad (2.1)$$

for which $\mu \ll 1$

When vortex excitation is included the differential equation becomes $\ddot{Y} + Y = \mu g(\tau, \dot{Y})$ (2.2)

and again $\mu \ll 1$.

The derivation of equations (2.1) and (2.2) is shown in the appendix. Both these equations are solved using the quasi-harmonic theory of Kryloff and Bogoliuboff[5]. The functions $f(\dot{Y})$ and $g(\tau, \dot{Y})$ were determined by approximating the lateral force coefficient (C_{Fy}) using Chebyshev polynomials[6]. For the models considered the respective coefficients of the polynomial are given in the appendix.

2.2 Differential Equation of First Kind

Consider

$$\ddot{Y} + Y = \mu f(\dot{Y})$$

when $\mu = 0$, the solution is of the form

$$Y = \bar{Y} \sin (\tau + \Phi) \tag{2.3}$$

$$\dot{Y} = \bar{Y} \cos (\tau + \Phi) \tag{2.4}$$

For $\mu \ll 1$ Kryloff and Bogoliuboff show that within a first approximation:

$$\frac{d\bar{Y}}{d\tau} = \mu f(\bar{Y} \cos(\tau + \Phi)) \cos (\tau + \Phi) \tag{2.5}$$

$$\frac{d\Phi}{d\tau} = -\frac{\mu}{\bar{Y}} f(\bar{Y} \cos (\tau + \Phi)) \sin (\tau + \Phi) \tag{2.6}$$

Since $\frac{d\bar{Y}}{d\tau}$, $\frac{d\Phi}{d\tau}$, are proportional to the small parameter μ, $\bar{Y}$ and Φ will be slowly varying functions of time during one period T. For the first approximation $\bar{Y}$ and Φ can be considered constant during one period. Let $\psi = \tau + \Phi$

Expanding $f(\bar{Y} \cos\psi) \cos\psi$, $f(\bar{Y} \cos\psi)\sin\psi$ in Fourier series, we have

$$f(\bar{Y} \cos\psi)\cos\psi = K_o(\bar{Y}) + \sum_{n>0} (K_n(\bar{Y})\cos n\psi)$$

$$f(\bar{Y} \cos\psi)\sin\psi = \sum_{n>0} (Q_n(\bar{Y})\sin n\psi) \quad \text{where}$$

$$K_o(\bar{Y}) = 1/2\pi \int_0^{2\pi} f(\bar{Y} \cos\psi) \cos\psi d\psi \tag{2.7}$$

and the coefficients K_n and Q_n are calculated in the usual way.

$$\frac{d\bar{Y}}{d\tau} = \mu(K_o(\bar{Y}) + \sum_{n>0} K_n(\bar{Y}) \cos n\psi)$$

$$\frac{d\Phi}{d\tau} = -\frac{\mu}{\bar{Y}} \sum_{n>0} Q_n(\bar{Y})\sin n\psi$$

Integrating these expressions in the interval t, t + T and considering $\bar{Y}$ and Φ to be constants within the interval, we arrive at the equations of the first approximation:

$$\frac{d\bar{Y}}{d\tau} = \mu K_o(\bar{Y}) \tag{2.8}$$

$$\frac{d\Phi}{d\tau} = 0 \tag{2.9}$$

These equations can also be written as $\frac{d\bar{Y}}{d\tau} = -\delta\bar{Y}$

where $$\delta = -\frac{\mu}{2\pi\bar{Y}} \int_0^{2\pi} f(\bar{Y}\cos\varphi)\cos\varphi d\varphi \tag{2.10}$$

and

$$\frac{d\varphi}{d\tau} = 1 - \frac{\mu}{2\pi\bar{Y}} \int_0^{2\pi} f(\bar{Y}\cos\varphi)\sin\varphi d\varphi = 1 \tag{2.11}$$

The stationary oscillations correspond to $\frac{d\bar{Y}}{d\tau} = 0$, and are therefore given by $\bar{Y} = 0$, and the real positive roots of the equation $\delta = 0$. In the phase plane, $\bar{Y} = 0$, the initial position of equilibrium, is a singular point at the origin known as a focus. The positive roots $\bar{Y}_i$ of equation $\delta = 0$ define trajectories in the phase plane known as limit cycles. The stability of equilibrium and of limit cycles is determined by investigating the tendency of the oscillator to return to the original focus or limit cycle after a small displacement.

The limit cycle is <u>stable</u> if

$$\frac{\partial\delta}{\partial\bar{Y}}\Big/_{\bar{Y}=\bar{Y}_i} > 0 \tag{2.12}$$

and <u>unstable</u> if

$$\frac{\partial\delta}{\partial\bar{Y}}\Big/_{\bar{Y}=\bar{Y}_i} < 0 \tag{2.13}$$

The model will not oscillate from rest if

$$\delta(0) > 0 \qquad (2.14)$$

However, self-excitation will take place if

$$\delta(0) < 0 \qquad (2.15)$$

The evaluations of $\frac{d\bar{Y}}{d\tau}$ and $\frac{d\Phi}{d\tau}$ terms for rectangular model cross-sections $(b/h = 2,\ b/h = 1/2)$ are shown in the appendix.

2.3 Differential Equation of Second Kind

Consider

$$\ddot{Y} + Y = \mu f(\dot{Y}) + Y_1 \sin(K_1\tau + \Phi_1) \qquad (2.16)$$

where $K_1 = \omega_1/\omega$ and Φ_1 constant

We distinguish two cases

1. $K_1 \neq 1$ (i.e.) Non-linear non-resonance
2. $K_1 \approx 1$ (i.e.) Non-linear external resonance

2.3.1 Non-Linear Non Resonance

Let $Y = x + \vartheta_1 \sin(K_1\tau + \Phi_1)$

where $\vartheta_1 = \dfrac{Y_1}{1-K_1^2}$

Substituting these in equation (2.16), we get

$$\ddot{x} + x = \mu f(\dot{x} + \vartheta_1 K_1 \cos(K_1\tau + \Phi_1)) \qquad \text{(i.e.) } \ddot{x} + x = \mu g(\tau, \dot{x})$$

As before when $\mu = 0$ $\quad x = \bar{Y}\sin(\tau + \Phi) = \bar{Y}\sin\psi$

$$\dot{x} = \bar{Y}\cos(\tau + \Phi) = \bar{Y}\cos\psi$$

Since $f(\dot{Y})$ is a polynomial in $\dot{Y}$ and $\dot{Y} = \dot{x} + \vartheta_1 K_1 \cos(K_1\tau + \Phi_1)$, then $g(\tau, \dot{x})$ is also a polynomial in $\dot{x}$.

Hence we can write

$$g(\tau, \dot{x}) = f_o(\dot{x}) + \sum_{n=1}^{M} f_n(\dot{x}) \cos nK_1\tau$$

As before from Kryloff and Bogoliuboff, we have

$$\frac{d\bar{Y}}{d\tau} = \mu \left[f_o(\bar{Y}\cos\psi) + \sum_{n=1}^{M} (f_n(\bar{Y}\cos\psi) \cos nK_1\tau) \right] \cos\psi$$

$$\frac{d\Phi}{d\tau} = -\frac{\mu}{\bar{Y}} \left[f_o(\bar{Y}\cos\psi) + \sum_{n=1}^{M} f_n(\bar{Y}\cos\psi) \cos nK_1\tau \right] \sin\psi$$

The Fourier expansions of f_o, f_n are

$$f_o(\bar{Y}\cos\psi) = \sum_{K\geq 0}^{M'} (g_K(\bar{Y})\cos K\psi)$$

$$f_n(\bar{Y}\cos\psi) = \sum_{K\geq 0}^{M'} (g_{n,K}(\bar{Y})\cos K\psi)$$

For the first approximation by the method of Kryloff and Bogoliuboff, we get

$$\frac{d\bar{Y}}{d\tau} = \mu \frac{1}{2\pi} \int_0^{2\pi} f_o(\bar{Y}\cos\psi) \cos\psi d\psi \qquad (2.18)$$

$$\frac{d\Phi}{d\tau} = -\frac{\mu}{2\pi\bar{Y}} \int_0^{2\pi} f_o(\bar{Y}\cos\psi) \sin\psi d\psi = 0 \qquad (2.19)$$

The expression for particular cases is given in the appendix.

2.3.2 Non-Linear External Resonance

For $K_1 \approx 1$

The equation (2.16) can be written in the form

$$\ddot{Y} + Y = \mu F(K_1\tau, \dot{Y})$$

By Kryloff and Bogoliuboff the generating solution is

$$Y = \bar{Y} \sin(K_1\tau + \Phi)$$

Let $K_1\tau + \Phi = \psi$

$$Y = \bar{Y} \sin\psi$$

Replacing the non-linear excitation force $e = \mu F(K_1\tau, \dot{Y})$ by the equivalent linear one

$e_1 = -\bar{\lambda}\dot{Y} - \bar{K}Y$ the D.E. becomes $\ddot{Y} + \bar{\lambda}\dot{Y} + \bar{K}Y = 0$

For the first approximation the equivalent parameter is obtained by equating the fundamental harmonic of $e = \mu F(K_1\tau, \bar{Y}K_1 \cos(K_1\tau + \Phi))$ to the linearized form

$e_1 = -\bar{\lambda}\bar{Y} K_1 \cos(K_1\tau + \Phi) - \bar{K}\bar{Y} \sin(K_1\tau + \Phi)$, where

$$\bar{\lambda} = -\frac{\mu}{\pi \bar{Y} K_1} \int_0^{2\pi} F((\psi - \Phi + \Phi_1), K_1\bar{Y}\cos\psi)\cos\psi \, d\psi$$

$$\bar{K} = -\frac{\mu}{\pi \bar{Y}} \int_0^{2\pi} F((\psi - \Phi + \Phi_1), K_1\bar{Y}\cos\psi)\sin\psi \, d\psi$$

The Kryloff and Bogoliuboff first approximation solution for this linearized equation is derived in the appendix.

III. APPARATUS AND INSTRUMENTATION

3.1 General Outline

From previous experiments on aeroelastic instability of bluff bodies, information was available on some of the problems to be encountered. Most of the equipment designed by Smith[2] was tested and found to be satisfactory for use in this project.

Force measurements on models were taken on the Aerolab strain gauge balance. A special bracket was made for mounting the model on the turntable of the balance.

Since Smith's displacement transducer needed to be calibrated for different ranges of amplitude a scale divided into 1/20 of an inch increments was mounted close to the shaft on the bottom floor of the tunnel. A D.C. differential amplifier with a gain of 60 was constructed for amplifying small amplitude displacements encountered in the vortex excited region. The amplifier output was recorded on a galvanometer-type chart recorder.

3.2 Wind Tunnel

All tests were performed in the University of British Columbia low speed, low turbulence, return-type tunnel in which velocity can be varied between 3 feet per second and 150 feet per second with a turbulence level of less than 0.1%. The flow is smoothed by three screens and enters the test section through a 7:1 contraction cone which accelerates the flow and improves its uniformity. The test section is 9 feet long, and has a cross section 36 inches by 27 inches, with 45° fillets. The fillets decrease from 6.0 inches at the upstream end to 4.75 inches at the downstream end to offset the effect of boundary layer growth.

The tunnel is powered by a 15 horsepower direct-current motor driving a commercial axial-flow fan with a Ward Leonard system of speed control. The pressure differential across the contraction is measured on a Betz micromanometer which can be read to 0.02 millimeter of water; the test section velocity is calibrated against the above pressure differential. The outline of the tunnel is given in fig (1).

3.3 Wind Tunnel Balance

Force measurements were taken from an Aerolab pyramidal strain gauge balance system. The balance system is designed to support a model in the wind tunnel, adjust its angle of attack over a ± 30 degree range, adjust its angle of yaw over a 360 degree range, and separate and measure the six force and moment components to determine the resultant force and moment exerted by the air stream on the model. The angular position of the model in yaw and angle of attack is indicated on Veeder Root Counters to the nearest tenth of a degree. The force components are separated mechanically and measured through individual strain gauge load cells. Read out is accomplished through the use of appropriate electrical equipment. Since the cylindrical models were mounted between the top and bottom of the tunnel the lift force and the angle of attack of the models were measured as side force and angle of yaw respectively on the balance. The balance was used only in measuring the lift and drag force of the models at different angles of attack.

The wind tunnel balance in position with the electrical read-out equipment is shown in fig.(2). A special bracket as shown in fig. (3) was made for attachment of the model to the "live" turntable.

The fairing turntable, with slots provided for model mounting and identical in dimension to the "live" turntable, was attached to the bottom panel of the wind tunnel. Filler blocks were used to cover the gap between the fairing turntable and the model.

3.4 Models

Static models used for force measurements were of "D" and rectangular cross section with end fittings provided to suit the turntable brackets of the wind tunnel balance. The "D" section was made from solid oak of two inch diameter, a smooth surface being obtained by spraying the model with acrylic plastic. The rectangular model was made out of solid aluminum of cross-section 1.870 inches by .935 inches. By using the yawing mechanism of the balance the rectangular section could be used as either b/h = 2 or b/h = 1/2, where "b" is the streamwise dimension and "h" is the width.

A dynamic model of rectangular cross section 1 inch by .5 inches by .065 inch wall thickness was made out of aluminum section with metal tabs provided at the ends for mounting. The end tabs could be rotated 90° degrees so that the model could be either used as b/h = 2 or b/h = 1/2. In order to investigate the dynamic behaviour of the model with splitter plate, Smith's b/h = 2 wooden model was used. The streamline model for damping calibration was made out of solid aluminum of cross section 1.4 inches by .15 inches; the corners were rounded

and slots were milled in the ends for mounting. Rectangular models for static and dynamic tests, and the streamline model are shown in fig.(4). The "D" section used for force measurements, with end fitting, is shown in fig.(3). Overall length of all the models used was 30 inches.

3.5 Model Mounting System

The mounting system used by Smith[2] was found to be adequate for the present investigation. It consists of two channels each supporting two air bearings at the top and bottom of the tunnel test section thus permitting only a plunging degree of freedom to the model. The top and bottom channels are connected by 2 1/2 inch x 2 1/2 inch angle iron bolted at the ends. Screws to adjust the parallelism of the two sets of bearings are located at the intersections of the lower channels and the angles. The lower channel can be moved in the stream direction to ensure that the model is vertical.

The air bearings support load by means of pressure forces caused by introducing high pressure air between the load carrying surfaces. High pressure air is introduced into the journal-type bearings through a number of equidistant holes around a circumference. Each of these holes contains a small regulating orifice. The air flows axially from the middle to the end of the bearings. The design and construction of the bearing is given by Smith[2].

Four springs were fastened to the top and bottom of the two angles with adjustable hooks. Light soldered aluminum clamps provided attachment for the springs and the model, to the shaft. Details of

the clamp, and the general arrangement of the top air bearing mounting system are given in fig. (5).

Air for the bearings was supplied by an Ingersoll-Rand 2-stage compressor, Model 11 3/4 & 7 x 8 VHB-2, pumping into a 250 cubic foot storage tank. Air was carried from the tank by a flexible hose to a throttling valve which distributed air at 60 pounds per square inch to all bearings from the main supply at 118 pounds per square inch.

3.6 Splitter Plate Mounting

Vertical streamwise splitter plates were connected to the top and bottom of the tunnel by 1 1/2 inch by 1 1/2 inch "handy angles". The connection of the angles to the tunnel floor and ceiling and the plate is shown in fig. (6). The plates were .0625 inch thick and 26.75 inches long. The plates were wide enough that the flow reattached on the plate after initial separation at the corners of the model. Arie and Rouse[7] found experimentally for a flat plate model of 3.0" by .0625" mounted transversely to the flow, a splitter plate of length 30" was necessary for the flow to reattach behind the model, thus preventing the formation of the alternating vortices in the wake. Plates of different widths of 6 inches, 5 inches, 4 inches, 3 inches, and 1 inch were made. The 6 inch plate was mounted as close as possible to the trailing edge of the model without touching it. Different widths of splitter plates were added to the 6 inch plate. It was found that an additional 4 inch plate was necessary for the flow reattachment to occur. The flow was assumed to have reattached when there was not an appreciable vibration of the plate with the wind on.

However, at large wind velocities the plate did vibrate and hence it was stayed to both sides of the wind tunnel side panel. The splitter plate in position behind the b/h = 2 wooden model with stays is shown in fig. (6).

3.7 Displacement Measurements

Displacement measurements were made with Smith's displacement transducer. It is essentially an air core transformer with primary and secondary coils wound on co-axial cylindrical forms with an annular gap between them. Either the inner or outer coil may be used as the primary winding. By inserting the aluminum shaft into the annulus, the magnetic coupling between the coils is varied, hence the output of the transducer is proportional to the displacement of the shaft. The displacement transducer was mounted on the top channel of the air bearing mounting system as shown in fig. (5). A 10 kc signal was used as the input to the primary windings of the transducer, using a Hewlett-Packard 202 C oscillator for excitation. The output signal of the transducer was a high-frequency carrier, amplitude modulated by displacement.

A full-wave rectifier with an appropriate filter used by Smith[2] was modified for demodulating the high frequency signal. A Minneapolis Honeywell Model 916 Visicorder was used to record the dynamic displacement and to record time-amplitude traces.

The galvanometer for this recorder has an input impedance of about 35 ohms and requires a source resistance of 3-100 ohms. Since

the transducer had a very high output impedance the output signal from the rectifier could not be directly fed into the recorder without seriously loading the transducer and affecting its performance. A D.C. differential amplifier was constructed to affect the matching. The amplifier built is used extensively in polar-cardiographs. Basic design characteristics were given by Hilbiber[8]. It had a gain of 60, input impedance of 2 megohms and an output impedance of 20 ohms. The schematic diagram for the amplifier is shown in fig. (7) and the amplifier in fig. (8).

The output signal from the rectifier had a D.C. level superimposed on the A.C. signal. To make use of the full six inch chart on the visicorder, a variable bias circuit was added to the rectifier. The schematic diagram of the rectifier with variable bias control is shown in fig. (9).

For calibration of the transducer a wooden scale marked in 1/20th of an inch increments was mounted close to the shaft under the floor of the wind tunnel as shown in fig. (10). When the model was oscillating a strobotachometer was used to give a clear indication of the shaft displacement.

3.8 Magnetic Damping

Damping, in addition to inherent damping within the system, was introduced by means of Smith's[2] electromagnetic eddy-current dampers. The model-carrying shafts pass through the magnetic field created by the damper. Energy is dissipated from the oscillating system by the

eddycurrents induced in the shafts.

There was an appreciable build up of residual magnetism on the damper probably due to the vibration of the tunnel at large amplitudes of model oscillation. To overcome this undesirable residual magnetism a system was arranged whereby the coils of the damper could be switched over to a variable A.C. source. The A.C. voltage is raised to give a greater magnetic field than the D.C. source had given, and then slowly decreased, effectively erasing the residual magnetism. The damping was found to be almost viscous for model amplitudes of .5 inches up to 5 inches. Position of the bottom damper is shown in fig.(10), and the electric supply circuit is given in fig.(11).

IV. TEST PROCEDURE AND RESULTS

4.1 Test Procedure

4.1.1 Static Tests

Static force measurements were taken on models of both rectangular cross section (b/h = 2, b/h = 1/2) and "D" section. The bottom end of each model was attached to the turntable of the balance and the balance was raised to a height such that the top end of the model had a clearance of .03 inches from the wind tunnel ceiling. Using the yawing mechanism of the balance, the angle of attack of the model could be varied by increments of $\pm$. 1 degree.

Due to the symmetry of the model section at zero angle of attack, no lift force was produced and this aerodynamic characteristic was used to establish the turntable position which gave zero angle of attack. At each angle of attack the balance bridge circuits for lift and drag components were set to a null position at zero wind speed; the lift and drag forces were recorded for various desired wind speeds. After each set of readings at one angle of attack, the zeros of the force recording channels were checked with no wind and found to be within $\pm$ 1% of the reading.

The angle of attack of the model was increased by increments of two degrees until complete flow reattachment occurred. In the region for which sharp changes occurred in the force measurements, the angle of attack of the model was increased in steps of 0.5 degree. Lift measurements could be read to an accuracy of $\pm$ 2% of the reading, while drag forces could be measured to an accuracy of $\pm$ 5% - 8%. This decrease of accuracy was due to the effect of model vibration.

4.1.2 Damping Calibration

For the calibration of the damper it was necessary to have a record of the logarithmic decrement of the streamline model at a desired value of current. The decay of amplitude with time given by the displacement transducer was recorded by the visicorder. A schematic diagram of the circuit is shown in fig.(12). To show the oscillation cycle clearly, the visicorder was set at a speed of 1 inch per sec. A 1 cycle per second triangular wave from a Hewlett-Packard 202A low frequency generator, which had an output impedance of 40 ohms, was directly connected to one channel of the visicorder. This signal was used as the time base for the amplitude-time decay record. The residual magnetism in the damper was removed as outlined in section 3.8. By changing the output of the variable power supply, the current in the damper was set to a desired value. The output of the oscillator supplying the high frequency signal to the displacement transducer was set to give a full trace on the visicorder for the possible maximum amplitude of the model. The throttling valve for the airbearings was adjusted to give a pressure of 60 psi. The streamline model was allowed to oscillate from a known initial amplitude. From the record of amplitude-time decay, the ratio of amplitude to initial amplitude was plotted against time on a semi-log graph. This procedure was repeated at each damping level and corresponding damping constants were determined.

The test section and equipment are shown in fig.(13).

4.1.3 Velocity-Amplitude and Amplitude-Time Measurements

The circuit shown for recording the logarithmic decrement of the streamline model was used in recording steady-state amplitude of the model on the visicorder. Utilizing the linearity of the displacement transducer, the output signal of the visicorder was calibrated against model amplitude which could be measured by the scale mounted on the bottom of the tunnel. For the maximum amplitude the output of the oscillator was set to give a full six inches deflection on the visicorder. To make use of the full six inches of the visicorder chart, thus giving greater accuracy in measuring amplitudes, separate calibration curves were drawn for various ranges of wind velocity.

After the damping level had been set for the test, the throttling valve was adjusted to give a pressure of 60 psi for the air bearings.

The tunnel was started at minimum air speed and the velocity increased until the model oscillated from rest. At intervals of one minute the displacement was recorded by the visicorder until the model amplitude reached a steady-state. The steady-state amplitudes were recorded for increasing wind velocity up to the limit of the air bearing system. Several check points were taken over this region with decreasing wind velocity. The tunnel was set at the minimum wind velocity at which the model oscillated from rest. While the model was oscillating the wind velocity was decreased in small increments and the corresponding steady amplitude recorded until the model stopped.

Due to vibration created by large model amplitude, it was frequently necessary to erase the residual magnetism built up in the

dampers. This procedure is described in section 3.8.

In the case of the b/h = 1/2 model, a desired wind velocity was set and the model was given a known initial amplitude. The displacement was recorded on the visicorder as previously described.

The circuit used in measuring steady-state amplitude was used in recording the amplitude-time build-up curve. The 1 cycle per second triangular signal used in damping calibration was fed into one channel of the visicorder for time base calibration. For a desired wind velocity the model was allowed to oscillate at a steady-state amplitude. The amplitude was measured, as previously described and the input to the displacement transducer was adjusted so that the full available width of the visicorder record was equal to the double amplitude. The model was stopped by shutting off the air supply to the air bearing, and started by suddenly turning it on again.

4.2 Results

4.2.1 Force Measurements

Force measurements were taken on models of b/h = 2, b/h = 1/2, and "D" Section. For each model, the force measurements were taken for five Reynolds numbers in the range of interest by varying the wind velocity. The force coefficients are presented uncorrected for tunnel wall effects. The corrections, using expressions given by Whitbread[9] would decrease values for the 2:1 rectangle by about 5.5%, for the 1/2:1 rectangle by about 7% and the "D" section by about 6%.

(a) b/h = 2

The lift and drag for two Reynolds numbers are shown in fig. (14). Within the experimental error the measurements taken for Reynolds numbers between 20,000 and 40,000 were bounded by these two curves. There is good agreement with Brooks'[1] result fig.(15). The polynomial used for representing the lateral force coefficients in the differential equation along with the measured coefficients are shown in fig. (16).

(b) b/h = 1/2

The Reynolds number effect on the lift and drag for this model is small fig.(17). Lift and drag measured by Brooks[1] are 8% higher fig.(18). The measured lateral force coefficient approximated by the 11th order Chebychev polynomial is shown in fig.(19).

(c) "D" Section

The lift and drag for angles of attack between 36° and 60° are extremely dependent on Reynolds number. This effect is shown in fig.

(20) for the five Reynolds numbers in the range of interest. The measured values of lift and drag lie between Brooks[1] and Cheers[11] for angles of attack up to 40°. At angles of attack higher than 40° there is good agreement with Cheers. This comparison for R_n = 66,000 is shown in fig. (21). The lateral force coefficient curves are extremely dependent on Reynolds number, and an extremely high order polynomial is also required to approximate them.

It would be more convenient to represent this lateral force coefficient by some other type of function. The lateral force coefficient for the two Reynolds numbers of interest is shown in fig. (22).

4.2.2 Velocity Amplitude

(a) b/h = 2

Velocity-amplitude measurements were made on aluminum (1/2" x 1") and wooden (1" x 2") models.

Aluminum Model

Five desired damping levels were used for this model. The non-dimensionalized experimental result with the corresponding theoretical curve for three damping values is shown in fig. (23).

Wooden Model

Velocity-amplitude measurements were made at three desired damping levels. The non-dimensionalized experimental and theoretical result for this model is shown in fig. (24). This was repeated with the splitter plate mounted in the wake at the model centre line.

The non-dimensionalized experimental result is shown in fig. (25). There was a strong amplitude modulation at the lower wind velocities when the splitter plate was removed from the wake. The envelope of the amplitude modulation for three damping levels is shown in fig. (26). The modulation frequency is shown versus non-dimensionalized wind velocity for two damping levels in fig. (27).

The theoretical velocity-amplitude curves for various damping levels for both the wooden and aluminum model collapse on to a single curve when multiplied by a suitable parameter as suggested by Parkinson[4]. The single theoretical curve with the experimental data reduced in the same way is shown in fig. (28a) and fig. (28b).

(b) $b/h = 1/2$

This model did not oscillate from rest for any wind velocity. For different wind velocities the model was given a maximum initial amplitude. In all cases the model did not continue to oscillate. The theoretical curves for two damping levels are shown in fig. (29).

4.2.3 Time-Amplitude Result for A.R.2. Model

Time-amplitude curves were recorded on the visicorder for the wooden and aluminum models. To predict the theoretical time-amplitude curve for one wind velocity, the initial amplitude was taken to be the value given by the visicorder for that velocity; the final amplitude necessary to calculate the build-up time was taken to be 95% of the theoretical value predicted for that wind velocity. The theoretical and experimental time amplitude build-up curves for

the aluminum model for various wind velocities are shown in fig. (30). When $\tau\beta$ is plotted against $\frac{nA}{2\beta}$ U all the theoretical curves for aluminum and wooden models collapse on to a single curve for a given initial amplitude. These theoretical curves for two initial amplitudes with the experimental points for both the models are shown in fig. (31).

V. DISCUSSION OF RESULTS

5.1 Damping Calibration

For double amplitude greater than 1", the semi-log plot of amplitude ratio with time used in calculating the damping coefficient "r" was linear showing the pure viscous effect of the damper. The calibration curve for the damper is shown with Smith's calibration in fig. (32). The present calibration is lower by a constant value due to the reduction in thickness of the aluminum shaft used in the present investigation. A small difference could also be present due to the different streamline model used.

5.2 Rectangular 2:1 Model

5.2.1 Force Measurements

The force measurement shows that at $\alpha = 0$ the flow which separates at the upstream corners of the model is symmetrical about the model centreline and hence does not develop any lateral force. With increasing α, the lateral force increases due to the increased asymmetry of the separated shearlayers. The lateral force coefficient reaches the maximum value when the windward shearlayer re-attaches on the underside of the model. There is a small increase in the angle of attack at which reattachment occurs with increase in Reynolds number. For the range considered re-attachment occurs at $\alpha = 7°$ which shows good agreement with Brooks[1]. Parkinson[3] has shown that the angle of attack at which the flow reattachment occurs limits the maximum amplitude, hence to use the quasi-steady approach, it is important to obtain the aerodynamic force coefficients for a Reynolds number close to that of the oscillating

cylinder whose response is to be investigated or predicted. In the amplitude range considered there is very little Reynolds number dependence of force coefficient. The graph of force coefficient confirms the "soft" oscillatory characteristic for the 2:1 rectangle. The polynomial approximation to the force coefficient is within the accuracy of the experimental investigation.

5.2.2 Comparison of Experimental Amplitude-Velocity and Velocity-Time Curves with Theoretical Prediction Using Differential Equation of the First Kind

(a) Amplitude-Velocity

For large values of U the theoretical predictions for the aluminum model for the three damping levels show good agreement with the experimental results. Only the stable limit cycle is compared with the experimental results, since with the present apparatus it was impossible to give the model a known initial amplitude. The beginning and the end point of the unstable limit cycle shown dotted was determined experimentally, and the agreement with the theoretical value is poor. For large values of U, as the theory predicts, the experimental values for the three damping levels shown lie on parallel curves, but for U values less than 24 there is a general trend for the experimental curves to converge. For the lowest damping the unstable limit cycle does not appear, and the model starts to oscillate from rest for the wind velocity corresponding to the resonance frequency of the vortex formation in the wake, which is far removed from the velocity predicted by the quasi-steady

theory. The comparison of experimental results with theory in this region is poor for U less than eight. For U greater than 8 the experimental curve follows closely the theoretical curve predicted.

The experimental results for the wooden model for the two damping levels shown do not agree with the theoretical values predicted. Similar to the aluminum model for the lower damping, the model oscillated from rest for the wind velocity corresponding to the vortex resonance. Smith's results shown for two values of damping are 4 percent higher.

The splitter plate, used in an attempt to eliminate effects of the vortex formation in the wake, made the model oscillate from rest for three different wind velocities corresponding to the three damping levels set. Although these velocities did not correspond to the values predicted by the quasi-steady theory they were well removed from the vortex resonance wind velocity. The experimental curve does not show any agreement with the theory predicted using the force measurements on the model without the splitter plate. To make such a comparison, the force measurements should be taken on the model with the splitter plate in the wake, which is extremely difficult to do. Although no comparison could be made with the theory the splitter plate investigation proved that the velocity at which the model started to oscillate from rest was influenced by the vortex formation in the wake.

The amplitude modulation shown for the wooden model for the three damping levels when the splitter plate is removed shows clearly

the effect of the vortex formation in the wake. To make further analysis of this effect dynamic pressure distributions should be measured on the model to see the instantaneous effect of the vortex formation on the after-body of the section. The regular modulation frequency for two damping levels increases with wind speed, because the vortex frequency is increasing. This frequency is captured (made equal to) the frequency of the oscillating system for a range of wind speeds near resonance (when the vortex frequency for a stationary cylinder equals the system natural frequency), but for wind speeds enough above the resonant value, the vortex frequency again increases with wind speed. At first it lies close enough to the frequency of the oscillating system to produce the observed beat phenomenon. This agrees qualitatively with the theoretical linear forced oscillation prediction for the beat phenomenon.

The results for the aluminum and wooden model are plotted in a dimensionless form fig. (28) according to which, if the theory correctly predicted the phenomenon, all points would collapse into the single theoretical curve predicted. The three sets of data for which U_o is less than 10 all give curves starting from zero amplitude at a wind speed corresponding closely to the vortex resonance, indicating that the vortices not accounted for in the galloping theory are mainly responsible for its discrepancies. The experimental velocity of $\frac{nAU}{2\beta} = .35$ for which the model oscillates from rest for zero amplitude does not agree with the theoretical value predicted.

The vortex formation in the wake not accounted for in the theory could be the cause of such a discrepancy since the splitter plate investigation showed that there was a strong effect of wake vortices on this velocity. To find the exact mechanism which governs the initiation of oscillations, instantaneous dynamic pressure distributions around the model will have to be considered.

(b) Velocity-Time

The experimental results for four wind velocities fig.(30) on the aluminum model show good agreement with the build-up time predicted by the quasi-steady theory. The theoretical single collapsed amplitude build-curves fig.(31) for two assumed initial amplitudes, show good agreement with the experimental results. The theoretical curve predicts a higher build-up time than is necessary for the wooden model since there is a strong influence of vortex formation on this model.

5.3 Theoretical Results Using Differential Equation of the Second Kind

5.3.1 Non-Linear Non-Resonance ($K_1 \neq 1$)

The square prism requires only a seventh order polynomial to approximate the experimental force coefficients, which simplifies mathematical computation considerably, and it was used to investigate the quasi-steady non-linear non-resonance condition. The general expression to calculate the steady state solution for this model is shown

in appendix III. The steady state solution has terms in powers of ϑ_1, which is a function of lift coefficient, mass parameter, wind velocity and the Strouhal number and is given by $\vartheta_1 = \frac{nC_{L_{f\ell}}}{1/U^{2-(2\pi S)}}$. When ϑ_1 is set to zero; that is, when there is no response function, the expression for steady-state amplitude reduces to the solution for the differential equation of the first kind given by Parkinson[4]. Any change in the steady-state solution for the differential equation of the second kind only involves terms in powers of ϑ_1 and can be neglected if ϑ_1 is very much smaller than one. When U is large $\vartheta_1 = \frac{nC_{L_{f\ell}}}{-(2\pi S)^2}$. For rectangular cylinders $C_{L_{f\ell}}/(2\pi S)^2$ is a finite quantity of order 1 and the magnitude of ϑ_1 is determined by the mass parameter "n". For the rectangular cylinders tested in the wind tunnel n is of order 10^{-4} and hence ϑ_1 can be neglected. The steady-state solution then reduces to the solution given by the differential equation of the first kind.

The mass parameter "n" has order of magnitude one if the experiment is performed in a water tunnel with the same experimental conditions used in the wind tunnel. The general solution is given by;

$$Y = \bar{Y} \sin(\tau + \Phi) + \vartheta_1 \sin(K_1\tau + \Phi_1)$$

The steady-state amplitude $\bar{Y}$ calculated is shown in fig. (33), for various assumed $C_{L_{f\ell}}$ values. For $C_{L_{f\ell}}$ less than .5 we have curves

similar to that predicted for the model in the wind tunnel. The unstable limit cycle which is given by the S bend is not shown for the model in the water tunnel, since it has been pushed close to the origin and is extremely small in magnitude. The magnitude of $\bar{Y}$ decreases with increasing $C_{L_{fl}}$ values. For values of $C_{L_{fl}}$ greater than about .5 there is no oscillation given by the galloping phenomenon. The solution then is given by $\bar{Y} = \vartheta_1 \sin (K_1\tau + \Phi_1)$. This quenching of auto-periodic oscillation by the hetero-periodic oscillation is termed "Asynchronous Quenching" (Minorsky).[12]

The rectangular 2:1 model also exhibits the above phenomena and the theoretical predictions are shown in fig, (34).

Heine[10] gives an experimental value of $C_{L_{fl}}$ for the square and 2:1 cylinder as 2.2 and 1.1 respectively. If these values are used, the theory predicts no galloping oscillations for the square and rectangular 2:1 cylinder in water flow.

5.3.2 Non-Linear External Resonance ($K_1 \approx 1$)

The expression derived for the 2:1 rectangular model is shown in appendix 2.2.2. The expression for the stationary oscillation (equation 12) is a function of $C_{L_{fl}}$ and this equation was solved using arbitrary values for $C_{L_{fl}}$ in the range .1 up to 2. For all the values $C_{L_{fl}}$ considered the equation for stationary oscillation predicted no oscillation. The investigation was not carried any further

and it is possible that a more detailed analysis might give a different result which would show better agreement with the experimental results near the vortex excited region.

5.4 The Rectangular 1/2:1 and the "D" Section

For the rectangular 1:1/2 Model the quasi-steady theory as shown predicts an initial double amplitude of 5 3/4" for the model to become unstable. With the present experimental apparatus it was only possible to give the model an initial double amplitude of 5", which explained the inability to find the upper stable limit cycle predicted by the theoretical curve.

The force measurements for the "D" section show a previously unsuspected large Reynolds number dependence for high incidence, related apparently to changing re-attachment characteristics on the semi-circular after-body of the section. Pressure distributions around the model in this region will have to be investigated to explain such re-attachment mechanism.

VI CONCLUSIONS

From this investigation, it may be concluded:

1. Contrary to previous belief the dynamic behaviour of the 2:1 rectangle can be predicted using a quasi-steady approach for models which have a U_o value greater than 10.
2. The discrepancy between quasi-steady theory prediction and the experimental result for the 2:1 rectangular model which has a U_o value smaller than 10, for values of U close to the natural frequency of the system, is due to the wake vortices not accounted for in the galloping theory and not due to a hysteresis in the separation and reattachment angles during the oscillation cycle.
3. For the rectangular 2:1 model in air, the quasi-steady theory prediction with the added forcing function, for external non-linear non-resonance condition, does not show any significant change from the theory predicted by neglecting the forcing function.
4. The quasi-steady theory predicts that the rectangular 2:1 and the square cylinders which exhibit galloping oscillation in air flow will not gallop for similar conditions in water flow since the galloping oscillations are quenched by the alternating vortices formed in the wake.
5. The modulation frequency observed for the A.R.2. wooden model is the beat phenomenon which is present when the vortex Strouhal frequency is captured by the model frequency.

6. There is a small Reynolds number effect on the lift and drag forces of the rectangular 2:1 and 1/2:1 model.

7. For the "D" section in the range of Reynolds number considered, for angles of attack greater than 36° and less than 60° there is a large Reynolds number effect on the lift and drag forces due to the changing re-attachment characteristics on the semi-circular afterbody of the section.

8. The rectangular 1/2:1 model is a hard oscillator as predicted by the quasi-steady theory.

9. Although the splitter plate mounted on the wake centre line of the rectangular 2:1 wooden model prevented the vortex excitation, the model oscillation behaviour in the galloping region did not agree with the theoretical value predicted using the force measurements of the model without the splitter plate.

VII RECOMMENDATION FOR FUTURE WORK

The dynamic pressure distribution should be investigated around the 2:1 rectangular model, for U_o values less than 10, to explain the discrepancy with the quasi-steady theory near vortex-excited region. The quasi-steady analysis with the vortex excitation should be further investigated for the non-linear external resonance condition ($K_1 \approx 1$).

To investigate the oscillating characteristics of the 1/2:1 rectangle some mechanical device should be designed to give the model the large initial amplitude necessary. The air bearing system will have to be redesigned to allow large amplitudes predicted by the quasi-steady theory.

The oscillating characteristics of the rectangular 2:1 and the square prism should be investigated experimentally in water flow to verify the results predicted by the quasi-steady theory.

APPENDIX I

Definition of Force Coefficient

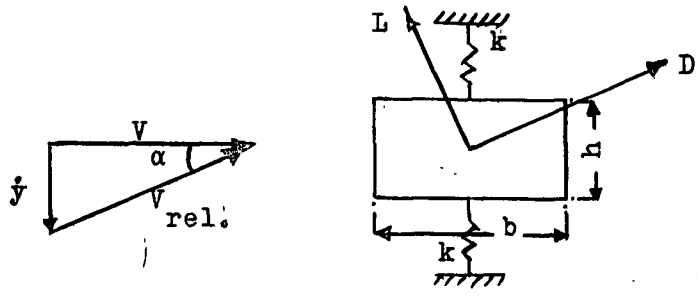

Define F_y as the aerodynamic force on the body, given by

$$F_y = -1/2 \rho V_{rel}^2 h \ell \, (C_L \cos \alpha + C_D \sin \alpha)$$

$$\text{but } V_{rel} = \frac{V}{\cos \alpha}$$

Therefore $F_y = -1/2 \rho V^2 h \ell (C_L + C_D \tan \alpha) \sec \alpha$

Define C_{F_y} by

$$C_{F_y} = F_y \, / \, 1/2 \rho V^2 h \ell$$

therefore $C_{F_y} = -(C_L + C_D \tan \alpha) \sec \alpha.$

APPENDIX II

2.1 Differential Equation of the First Kind for the Rectangular 2:1 Model

The differential equation of motion is

$$m\ddot{y} + r\dot{y} + ky = 1/2 C_{Fy} \rho V^2 h \ell \qquad (1)$$

Let $C_{Fy} = F(\dot{y}/V)^{11} - E(\dot{y}/V)^9 + D(\dot{y}/V)^7 - C(\dot{y}/V)^5 + B(\dot{y}/V)^3 + A(\dot{y}/V)$

where A,B,C,D,E,F are the coefficients of the polynomial used to approximate the experimental C_{Fy} curve using Chebyshev polynomials and are given by

$F = 572.79098 \times 10^5$ $\quad E = 160.73516 \times 10^5$

$D = 166.428 \times 10^4$ $\quad C = 742.39918 \times 10^2$

$B = 1100.6281$ $\quad A = 2.329066$

Substituting this in Equation 1 and non-dimensionalizing, we get

$$\ddot{Y} + Y = nA\left[\left(U - \frac{2\beta}{nA}\right)\dot{Y} + \frac{B}{AU}\dot{Y}^3 - \frac{C}{AU^3}\dot{Y}^5 + \frac{D}{AU^5}\dot{Y}^7 - \frac{E}{AU^7}\dot{Y}^9 + \frac{F}{AU^9}\dot{Y}^{11}\right] \qquad (2)$$

This is of the form discussed in Section 2.2, from which we get

$\mu = nA$,

$\frac{d\bar{Y}}{d\tau} = -\delta\bar{Y}$ where

$$\delta = -\frac{nA}{2}\left[\left(U - \frac{2\beta}{nA}\right) + \frac{3}{4}\frac{B}{AU}\bar{Y}^2 - \frac{5}{8}\frac{C}{AU^3}\bar{Y}^4 + \frac{35}{64}\frac{D}{AU^5}\bar{Y}^6 - \frac{63}{128}\frac{E}{AU^7}\bar{Y}^8 + \frac{231}{512}\frac{F}{AU^9}\bar{Y}^{10}\right] \qquad (3)$$

$\frac{d\varphi}{d\tau} = 1$ $\quad$ therefore Φ = constant

For steady-state solution

$$\frac{d\bar{Y}}{d\tau} = 0 \quad \text{i.e.,} \quad \delta = 0 \qquad (4)$$

If δ (0)< 0 self excitation will take place

(i.e.) if $U > \frac{2\beta}{nA} = U_o$

2.2. Differential Equation of the Second Kind for the Rectangular 2:1 Model

2.2.1 Non-Linear Non-Resonance:

The differential equation of motion is

$$m\ddot{y} + r\dot{y} + ky = 1/2\, C_{Fy} \rho V^2 h \ell + F_o \sin(\omega_1 t + \Phi_1) \qquad (5)$$

where $F_o = C_{L_{f\ell}}\, 1/2 \rho V^2 h \ell$; Φ_1 = some phase angle

Non-dimensionalizing this equation, we get

$$\ddot{Y} + Y = \mu f(\dot{Y}) + Y_1 \sin(K_1 \tau + \Phi_1) \qquad (6)$$

where $\mu = nA$, $\tau = \omega t$

$Y_1 = F_o / m\omega^2 h$, $K_1 = \frac{\omega_1}{\omega}$

Equation (6) is of the form discussed in Section 2.3.1

From which we get

$$\frac{d\bar{Y}}{d\tau} = -\delta_e \bar{Y} \qquad \frac{d\Psi}{d\tau} = 0$$

therefore Φ = constant

where

$$\delta_e = -\frac{\mu}{2}\left[\left\{(U - \frac{2\beta}{nA}) + \frac{3}{2}\frac{B}{AU}\vartheta_1^2 K_1^2 - \frac{15}{8}\frac{C}{AU^3}\vartheta_1^4 K_1^4 + \frac{35}{16}\frac{D}{AU^5}\vartheta_1^6 K_1^6 - \frac{315}{128}\frac{E}{AU^7}\vartheta_1^8 K_1^8 + \frac{693}{256}\frac{F}{AU^9}\vartheta_1^{10} K_1^{10}\right\}\right.$$

$$\left. + \left\{\frac{3}{4}\frac{B}{AU} - \frac{15}{4}\frac{C}{AU^3}\vartheta_1^2 K_1^2 + \frac{315}{32}\frac{D}{AU^5}\vartheta_1^4 K_1^4 - \frac{315}{16}\frac{E}{AU^7}\vartheta_1^6 K_1^6 + \frac{17325}{512}\frac{F}{AU^9}\vartheta_1^8 K_1^8\right\}\bar{Y}^2\right]$$

$$+\left\{-\frac{5}{8}\frac{C}{AU^3}+\frac{105}{16}\frac{D}{AU^5}\vartheta_1^2K_1^2-\frac{945}{32}\frac{E}{AU^7}\vartheta_1^4K_1^4+\frac{5775}{64}\frac{F}{AU^9}\vartheta_1^6K_1^6\right\}\bar{Y}^4$$

$$+\left\{\frac{35}{64}\frac{D}{AU^5}-\frac{630}{64}\frac{E}{AU^7}\vartheta_1^2K_1^2+\frac{17325}{256}\frac{F}{AU^9}\vartheta_1^4K_1^4\right\}\bar{Y}^6$$

$$+\left\{-\frac{63}{128}\frac{E}{AU^7}+\frac{3465}{256}\frac{F}{AU^9}\vartheta_1^2K_1^2\right\}\bar{Y}^8+\frac{231}{512}\frac{F}{AU^9}\bar{Y}^{10}\Bigg] \qquad (7)$$

and $\vartheta_1=\dfrac{Y_1}{1-K_1^2}$

The steady-state solution is given by

$$\frac{d\bar{Y}}{d\tau}=0 \quad \text{(i.e.)} \quad \delta_e=0$$

If δ in section 2.2 is replaced by δ_e, then all the stability analysis discussed there can be directly applied for this case.

2.2.2 $K_1\approx 1$ Non-Linear External Resonance

The solution to the linearized equation by Kryloff and Bogoliuboff for the first approximation is

$$Y=\bar{Y}\sin(K_1\tau+\Phi)=\bar{Y}\sin\psi \qquad (8)$$

Where $\dfrac{d\bar{Y}}{d\tau}=-\dfrac{\bar{\lambda}\bar{Y}}{2}$ (9)

$$\frac{d\Phi}{d\tau}=\sqrt{1+\bar{K}}-K_1$$

and $\bar{\lambda}=-\dfrac{1}{\pi\bar{Y}K_1}\displaystyle\int_0^{2\pi}\left[\mu f\left(\bar{Y}K_1\cos\psi\right)+Y_1\sin(\psi-\Phi+\Phi_1)\right]\cos\psi\,d\psi$ (10)

$$\bar{K} = -\frac{1}{\pi\bar{Y}} \int_0^{2\pi} \left[\mu f(\bar{Y} K_1 \cos\varphi) + Y_1 \sin(\varphi - \Phi + \Phi_1)\right] \sin\varphi \, d\varphi$$

$$= -\frac{1}{\pi\bar{Y}} \int_0^{2\pi} Y_1 \sin(\varphi - \Phi + \Phi_1) \sin\varphi \, d\varphi \qquad (11)$$

therefore $\bar{K} = -\frac{1}{\bar{Y}} Y_1 \cos(\Phi - \Phi_1)$

From equation (10)

$$-\frac{1}{\pi\bar{Y} K_1} \int_0^{2\pi} \mu f(\bar{Y} K_1 \cos\varphi) \cos\varphi \, d\varphi$$

$$\approx -\frac{1}{\pi\bar{Y}} \int_0^{2\pi} \mu f(\bar{Y} \cos\varphi) \cos\varphi \, d\varphi \qquad (\text{Since } K_1 \approx 1.)$$

$= 2\delta$ (For 2:1 rectangular model from equation 2.10)

Therefore $\bar{\lambda} = 2\delta - \frac{1}{\pi \bar{Y} K_1} \int_0^{2\pi} Y_1 \sin(\varphi - \Phi + \Phi_1) \cos\varphi \, d\varphi$

and $\frac{d\bar{Y}}{d\tau} = -(\delta + \frac{1}{2\bar{Y} K_1} Y_1 \sin(\Phi - \Phi_1))\bar{Y}$

From equation (9)

$$\frac{d\Phi}{d\tau} = \sqrt{1 + \bar{K}} - K_1 \approx 1 + \frac{\bar{K}}{2} - K_1$$

therefore $\frac{d\Phi}{d\tau} = 1 - \frac{Y_1}{2\bar{Y}} \cos(\Phi - \Phi_1) - K_1$

For stationary oscillations $\frac{d\bar{Y}}{d\tau} = \frac{d\Phi}{d\tau} = 0$

Therefore Equations (8) and (9) reduce to

$$1 - \frac{Y_1}{2\bar{Y}} \cos(\Phi - \Phi_1) - K_1 = 0$$

$$\delta + \frac{1}{2\bar{Y}K_1} Y_1 \sin(\Phi - \Phi_1) = 0$$

Let $K_1 = 1$ (at resonance). Then

$$\cos^2(\Phi - \Phi_1) = 0$$

$$\sin^2(\Phi - \Phi_1) = \left(\frac{-2\delta\bar{Y}}{Y_1}\right)^2 = \frac{4\delta^2\bar{Y}^2}{Y_1^2} \qquad (12)$$

therefore $\bar{Y} = Y_1/2\delta$

where $Y_1 = nU^2 C_{L_{f\ell}}$

APPENDIX III

Non-Linear Non-Resonance for a Square Section

The differential equation is given by

$$\ddot{Y} + \dot{Y} = nA\left(U - \frac{2\beta}{nA}\right)\dot{Y} - \left(\frac{B}{AU}\right)\dot{Y}^3 + \left(\frac{C}{AU^3}\right)\dot{Y}^5 - \left(\frac{D}{AU^5}\right)\dot{Y}^7 + Y_1 \sin\left(K_1\tau + \Phi_1\right)$$

where for a Reynolds number of 22,000, the coefficients of the polynomial are given as A = 2.69, B = 168, C = 6270, D = 59,900.

The general solution is of the form

$$Y = \bar{Y} \sin\left(\tau + \Phi\right) + \vartheta_1 \sin\left(K_1\tau + \Phi_1\right)$$

For steady-state amplitude

$$\frac{d\Phi}{d\tau} = 0 \text{ i.e. } \Phi = \text{a constant}$$

and $ax^3 + bx^2 + cx = d$

where

$$x = \left(\bar{Y}/U\right)^2$$

$$a = \frac{35}{64}\frac{D}{A}$$

$$b = -\frac{5}{8}\frac{C}{A} + \frac{105}{16}\frac{D}{A}\left(2\pi\vartheta_1 S\right)^2$$

$$c = \frac{3}{4}\frac{B}{A} - \frac{15}{4}\frac{C}{A}\left(2\pi\vartheta_1 S\right)^2 + \frac{315}{32}\frac{D}{A}\left(2\pi\vartheta_1 S\right)^4$$

$$d = \left(1 - \frac{2\beta}{nAU}\right) - \frac{3}{2}\frac{B}{A}\left(2\pi\vartheta_1 S\right)^2 + \frac{15}{8}\frac{C}{A}\left(2\pi\vartheta_1 S\right)^4 - \frac{35}{16}\frac{D}{A}\left(2\pi\vartheta_1 S\right)^6$$

$$S = \frac{\omega_1 h}{2\pi V} = \frac{K_1}{2\pi U}$$

APPENDIX IV

Differential Equation of the First Kind for the Rectangular 1/2:1 Model

The differential equation of motion is

$$m\ddot{y} + r\dot{y} + ky = 1/2\ C_{Fy}\rho V^2 h\ell$$

where

$$C_{Fy} = F(\dot{y}/V)^{11} - E(\dot{y}/V)^9 + D(\dot{y}/V)^7 - C(\dot{y}/V)^5 + B(\dot{y}/V)^3 - A(\dot{y}/V)$$

$F = 656.12104 \times 10^2$ $E = 375.25079 \times 10^2$ $D = 7076.95$

$C = 503.36067$ $B = 15.72543$ $A = .27513333$

The expression used in Appendix 2.1 can be directly used for calculating steady-state amplitude when the coefficients are replaced by the above coefficients and the $\dot{y}/V$ term of the C_{Fy} polynomial is replaced by a negative sign.

BIBLIOGRAPHY

1. Brooks, N.P.H. "Experimental Investigation of Aeroelastic Instability of Bluff Two-Dimensional Cylinders." M.A.Sc. Thesis, University of British Columbia, July, 1960.

2. Smith, J.D. "An Experimental Study of the Aeroelastic Instability of Rectangular Cylinders." M.A.Sc. Thesis, University of British Columbia, August 1962.

3. Parkinson, G.V. "Aeroelastic Galloping in One Degree of Freedom", Proc. Int. Conf. on Wind Effects on Bldgs. and Structures, London, 1965.

4. Parkinson, G.V. "The Square Prism as an Aeroelastic Non-Linear Oscillator" Quarterly Journal of Mechanics and Applied Mathematics, Volume XVll Part 2, May 1964.

5. Kryloff, N. and Bogoliuboff, N. "Introduction to Non-Linear Mechanics." Translation by Solomon Lefschetz of Excerpts from Two Russian Monographs.

6. "Tables of Chebyshev Polynomials" U.S. National Bureau of Standards, App. Math. Series 9, December 1952.

7. Arie, M. and Rouse, H. "Experiments on Two-Dimensional Flow Over a Normal Wall." Journal of Fluid Mechanics, Volume I. 1956

8. Hilbiber, D.F. "A New D-C Transistor Differential Amplifier." 1962 Fairchild Semi-conductor TP - 16.

9. Whitbread, R.E. "Model Simulation of Wind Effects on Structures", Proc. Int. Conf. on Wind Effects on Bldgs. and Structures, London, 1965.

10. Heine, W. "The Experimental Investigation of Vortex Excited Pressure Fluctuations", M.A.Sc. Thesis University of British Columbia, August 1964.

11. Cheers, F. "A Note on Galloping Conductors", National Research Council of Canada Report No. MT-14. 1950.

12. Minorsky, N. "Introduction to Non-Linear Mechanics", Edwards Brothers, Inc. 1947.

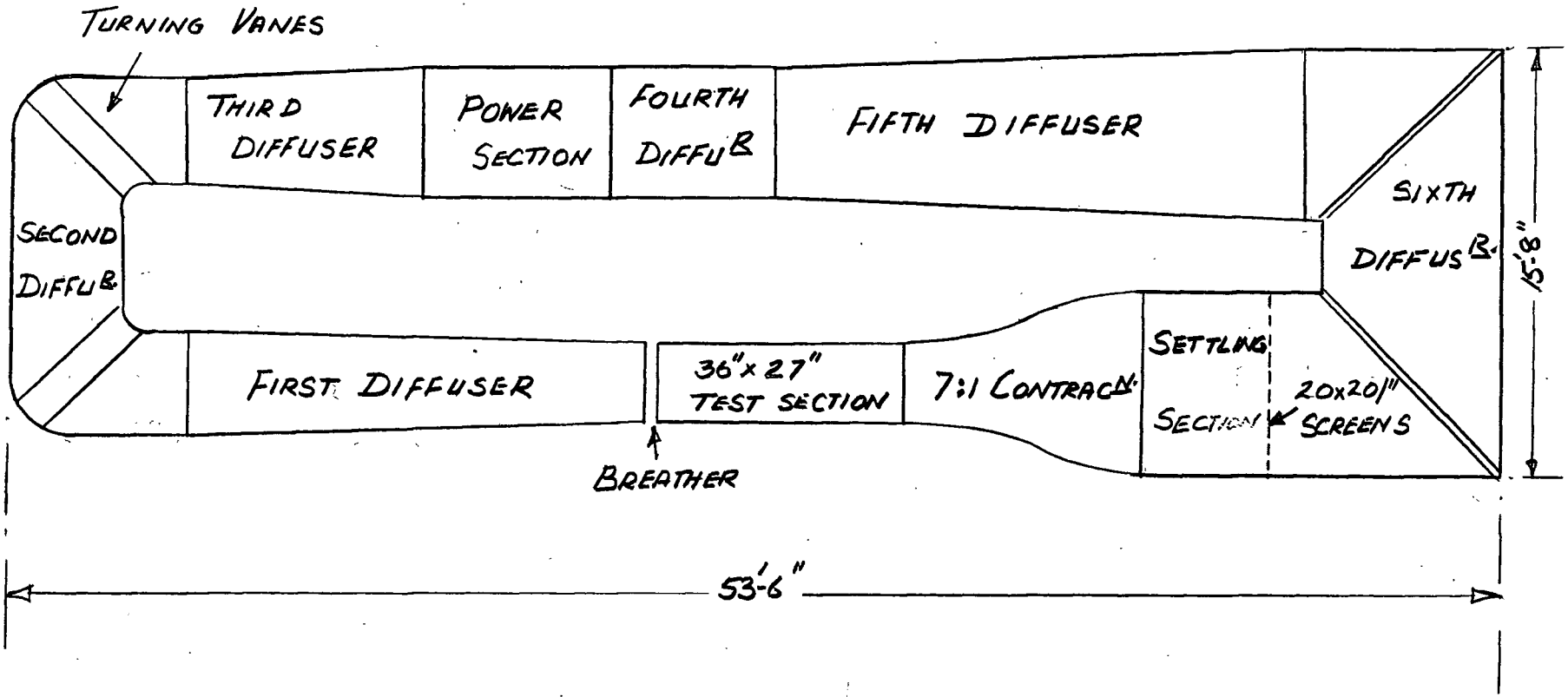

Fig. (1) Wind Tunnel Aerodynamic Outline

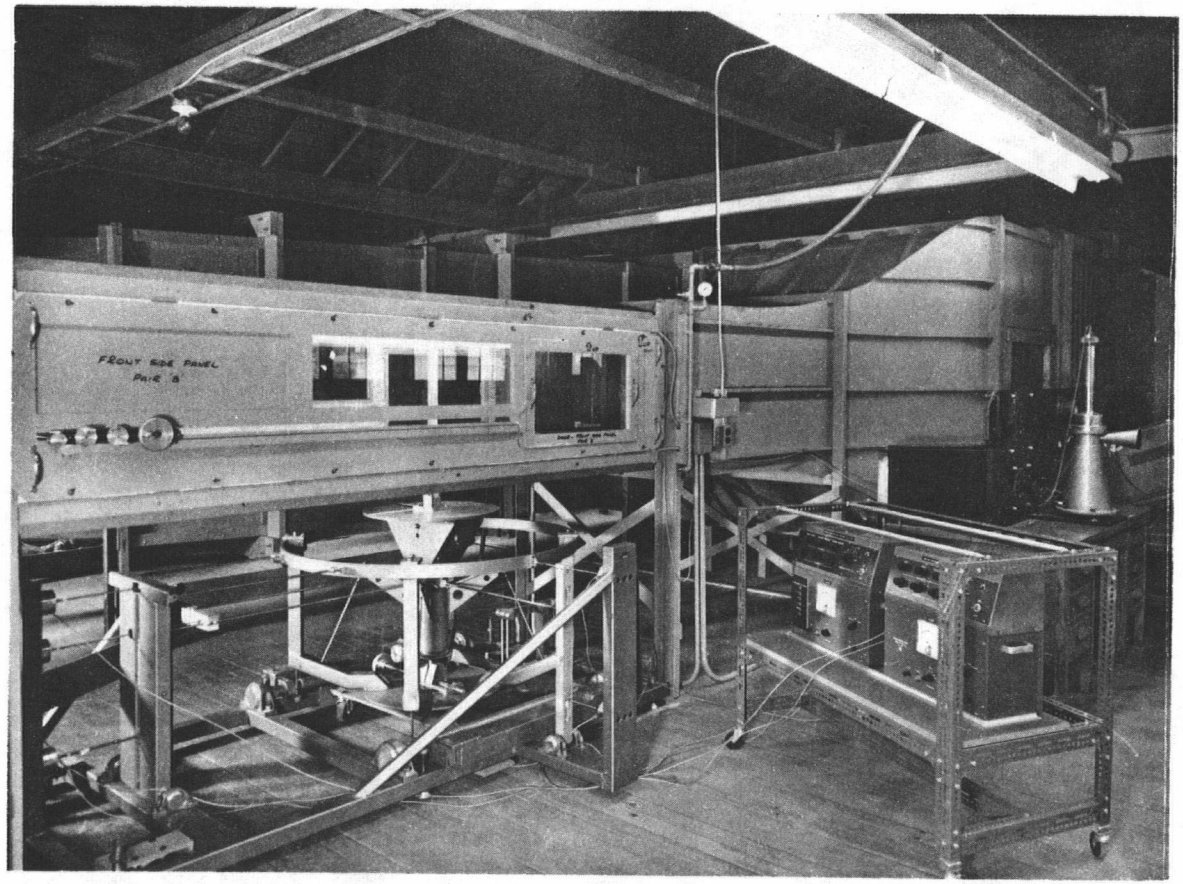

Fig. (2) Wind Tunnel Balance in Position

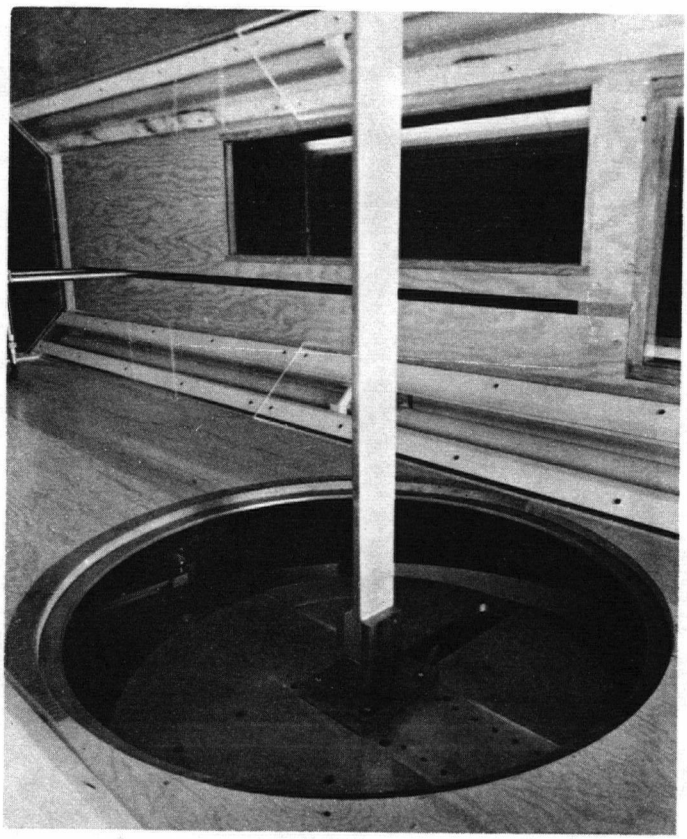

Fig. (3) D - Section Model Mounted on Turntable

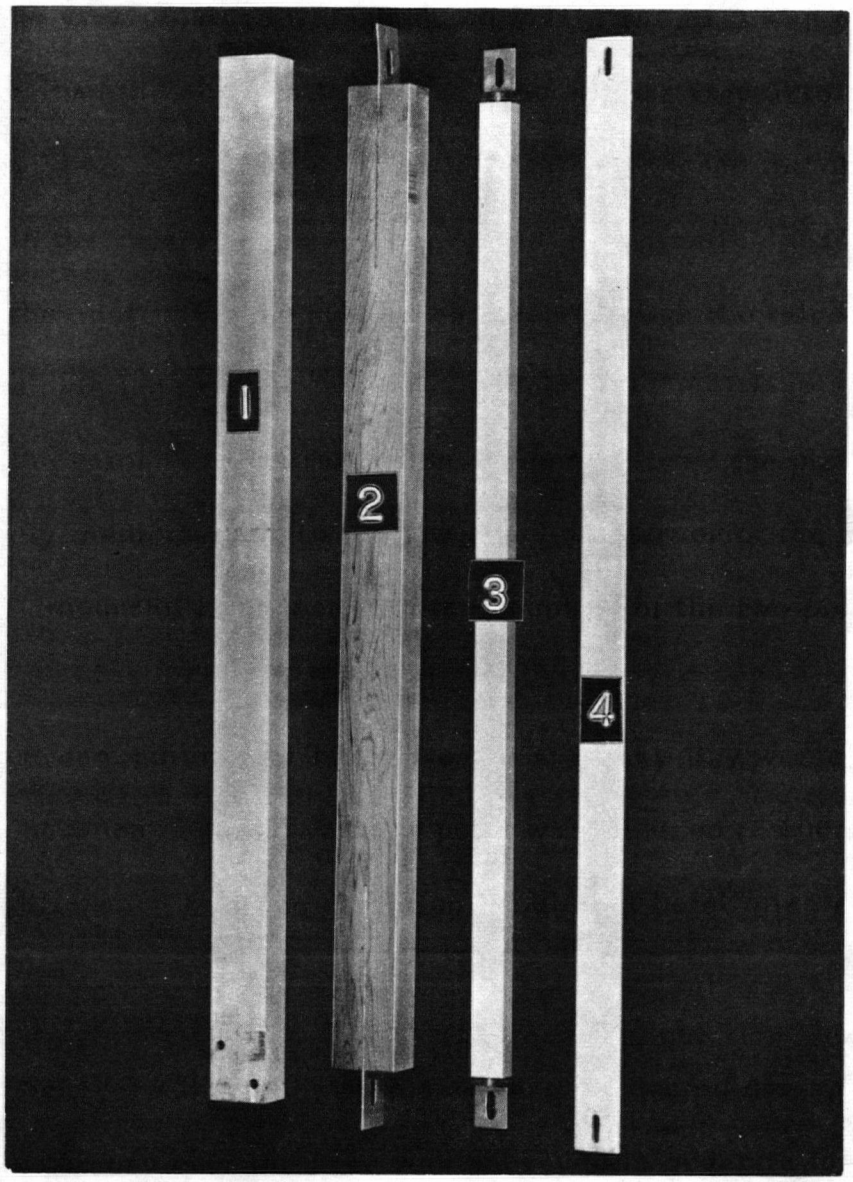

1. Rectangular Static Model
2. Dynamic A.R.2 Wooden Model
3. Dynamic A.R.2 and A.R. 1/2 Aluminum Model
4. Streamline Model

Fig. (4) Test Models

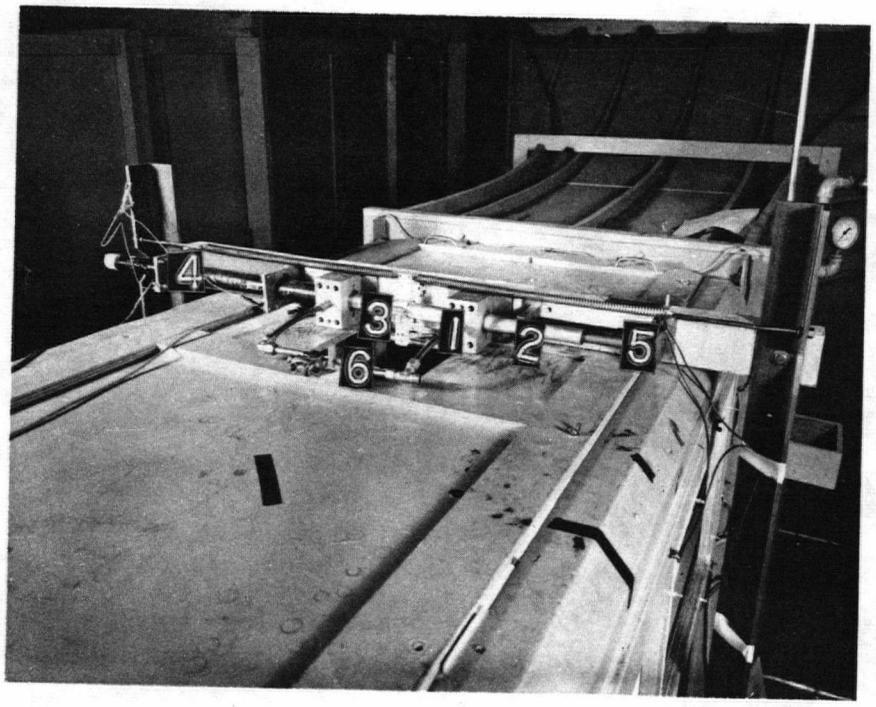

1. Air Bearing
2. Aluminum Shaft
3. Model Clamp
4. Displacement Transducer
5. Damper
6. Compressed Air Supply

Fig. (5) General Arrangement of the Top Air Bearing System

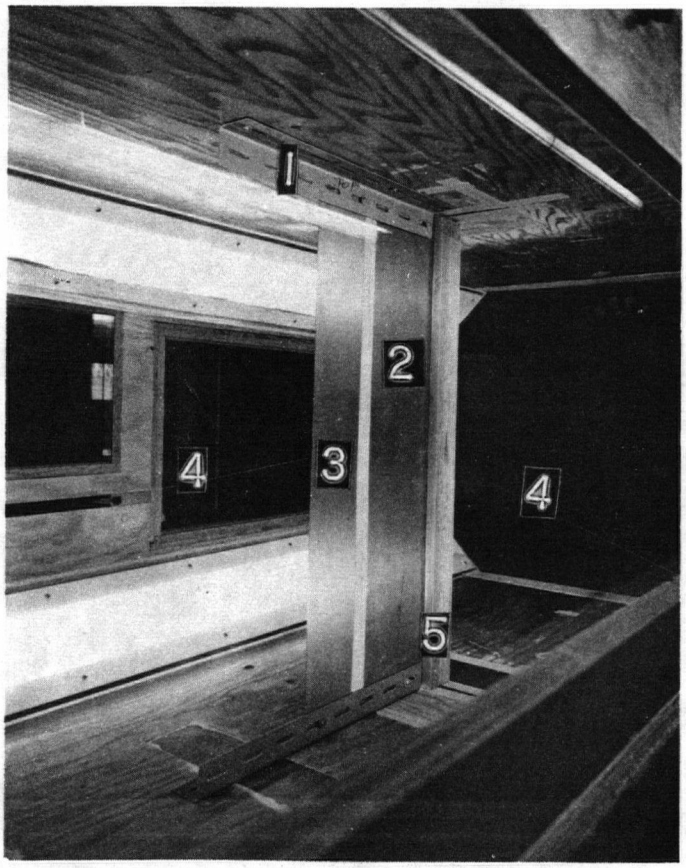

1. Handy Angles
2. Basic 6 " Splitter Plate
3. Additional 4" Splitter Plate
4. Stay Wires
5. A.R. 2 Wooden Model

Fig. (6) Model Mounted with Splitter Plate

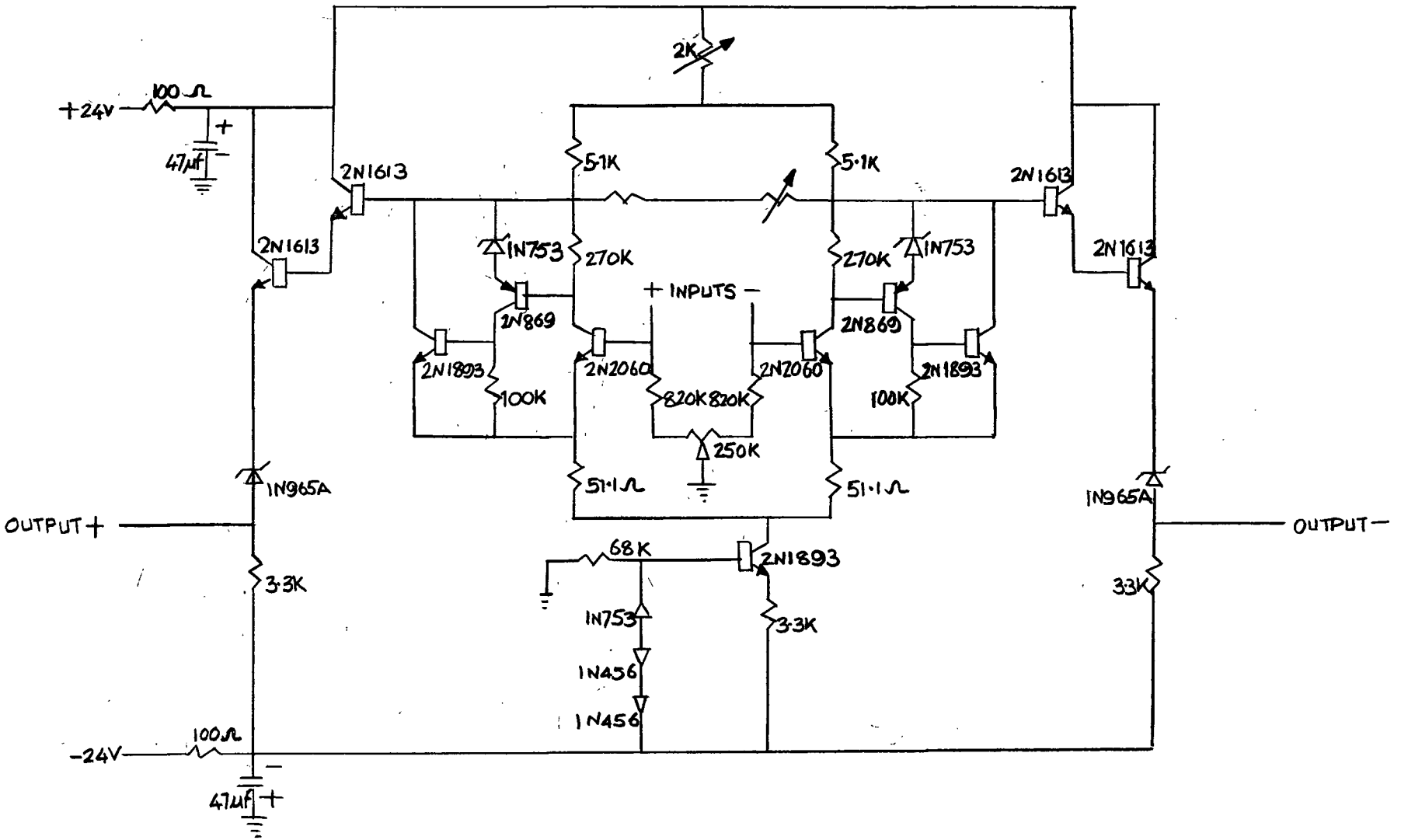

Fig. (7) D.C. Differential Amplifier

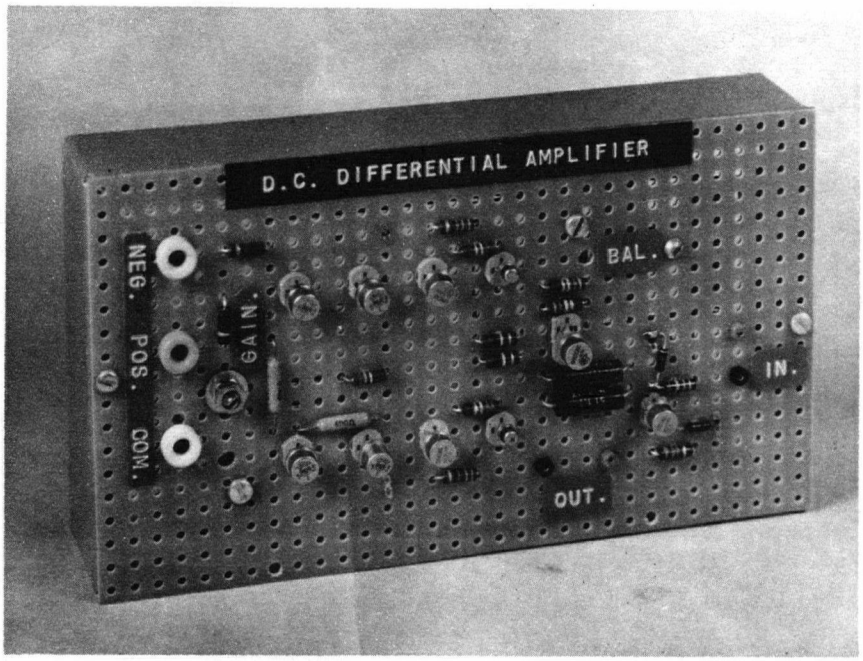

Fig. (8) D.C. Differential Amplifier

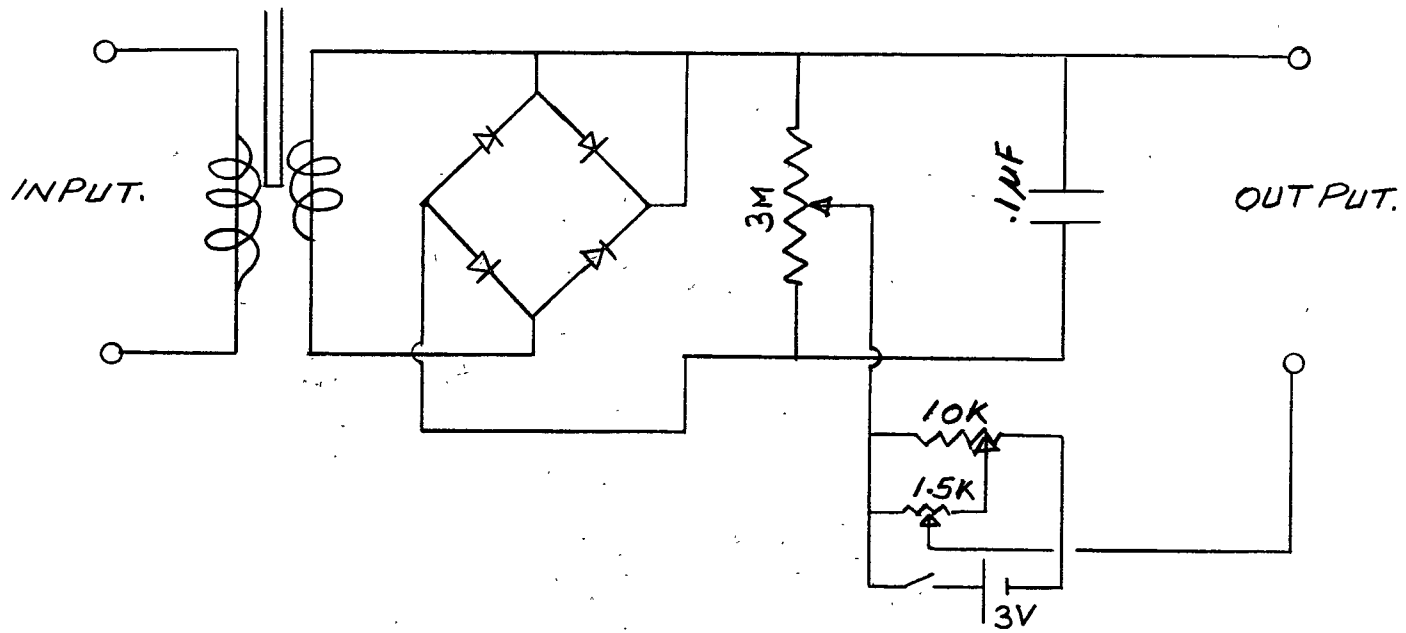

Fig. (9) Rectifier and Bias Unit

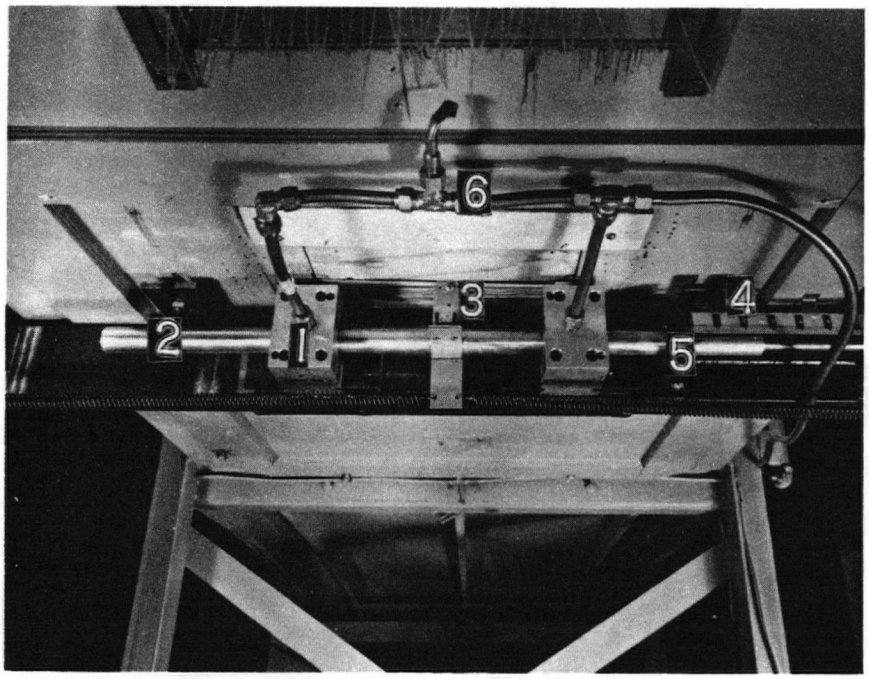

1. Air Bearings
2. Aluminum Shaft
3. Model Clamps
4. Calibrating Scale
5. Damper
6. Compressed Air Supply

Fig. (10) General Arrangement of the Bottom Air Bearing System

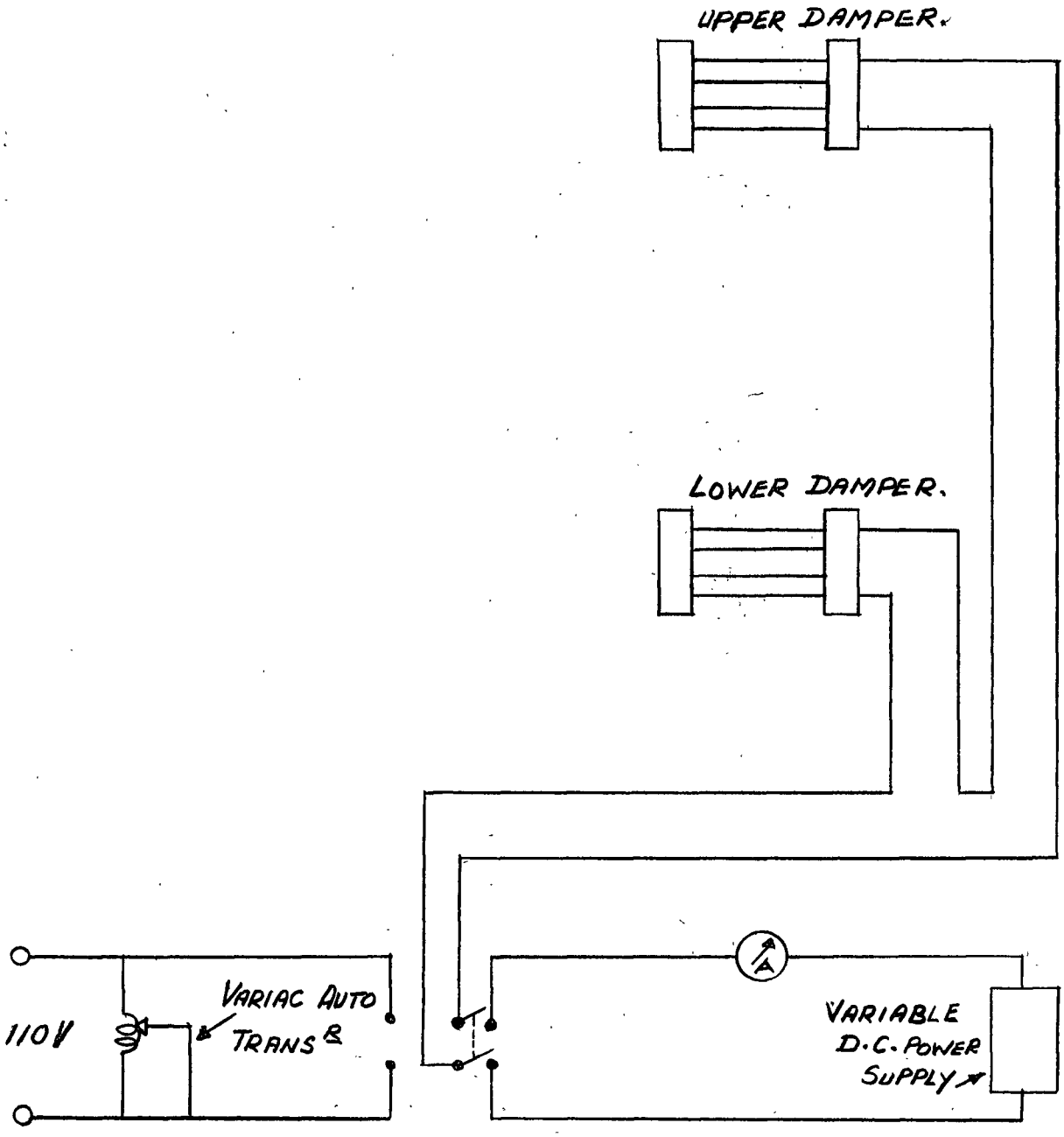

Fig. (11) Damper Circuit

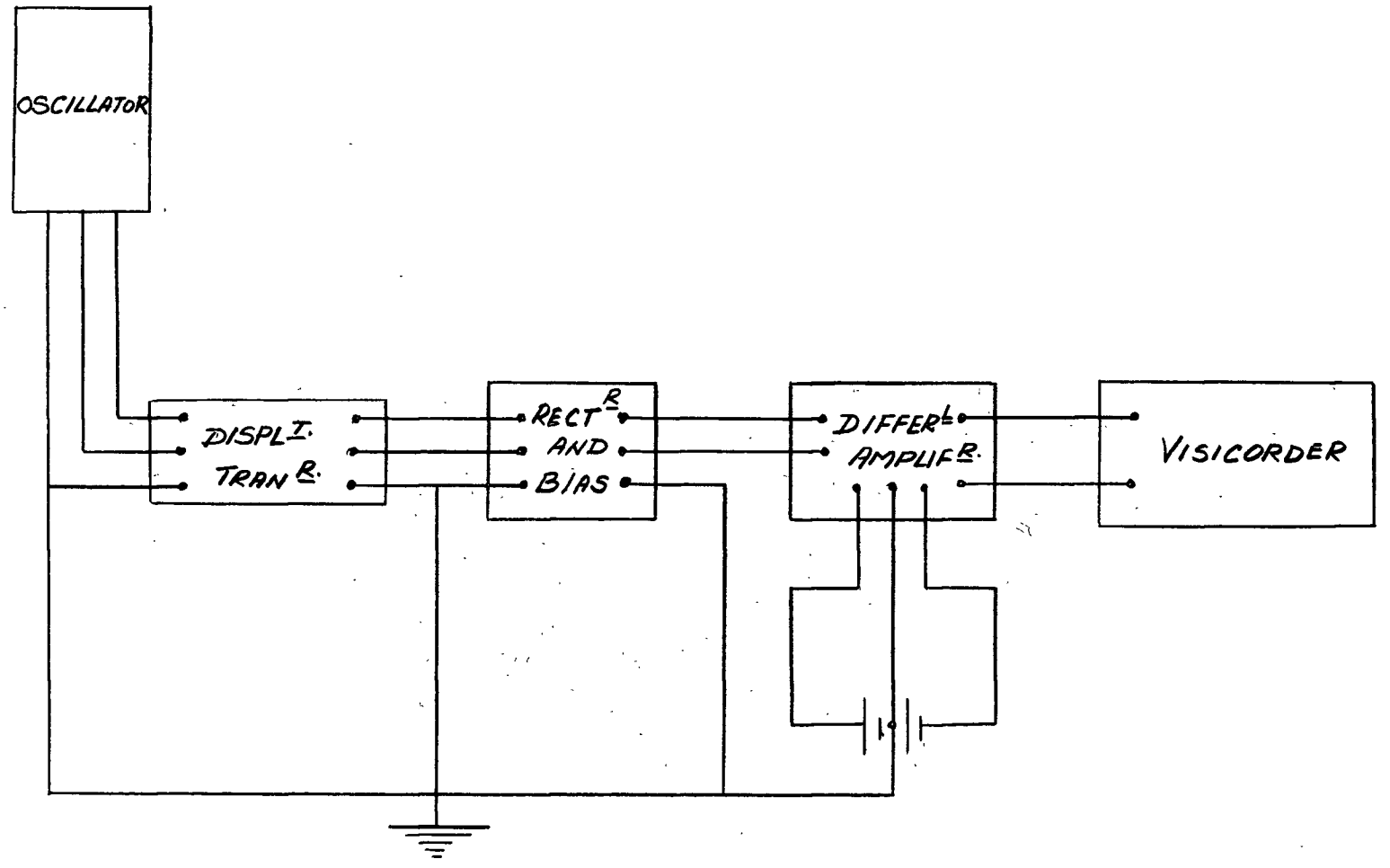

Fig. (12) Displacement Measurement Instrumentation

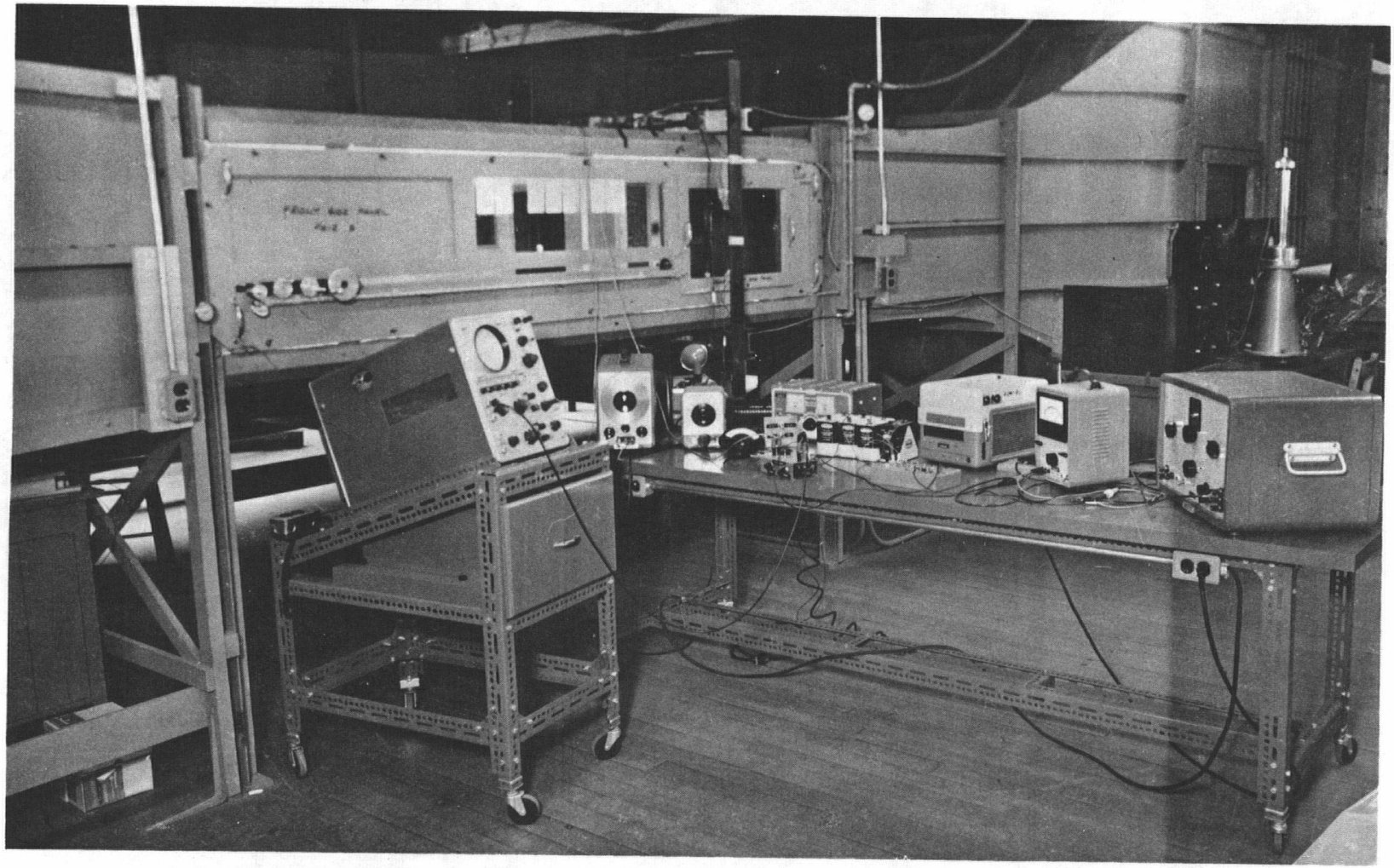

Fig. (13) Test Section and Equipment

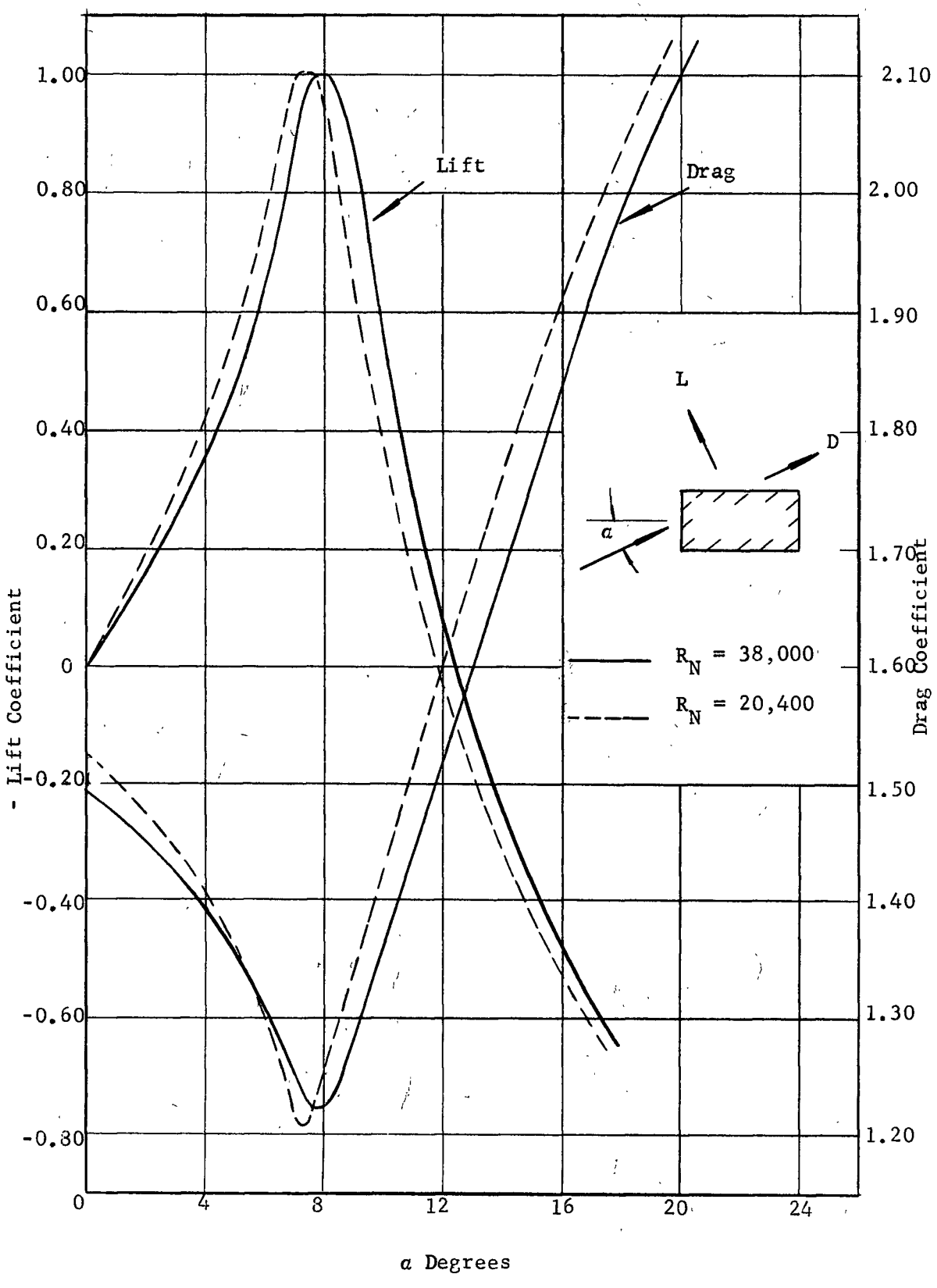

Fig. (14) Sectional Lift And Drag Coefficient for 2:1 Rectangle

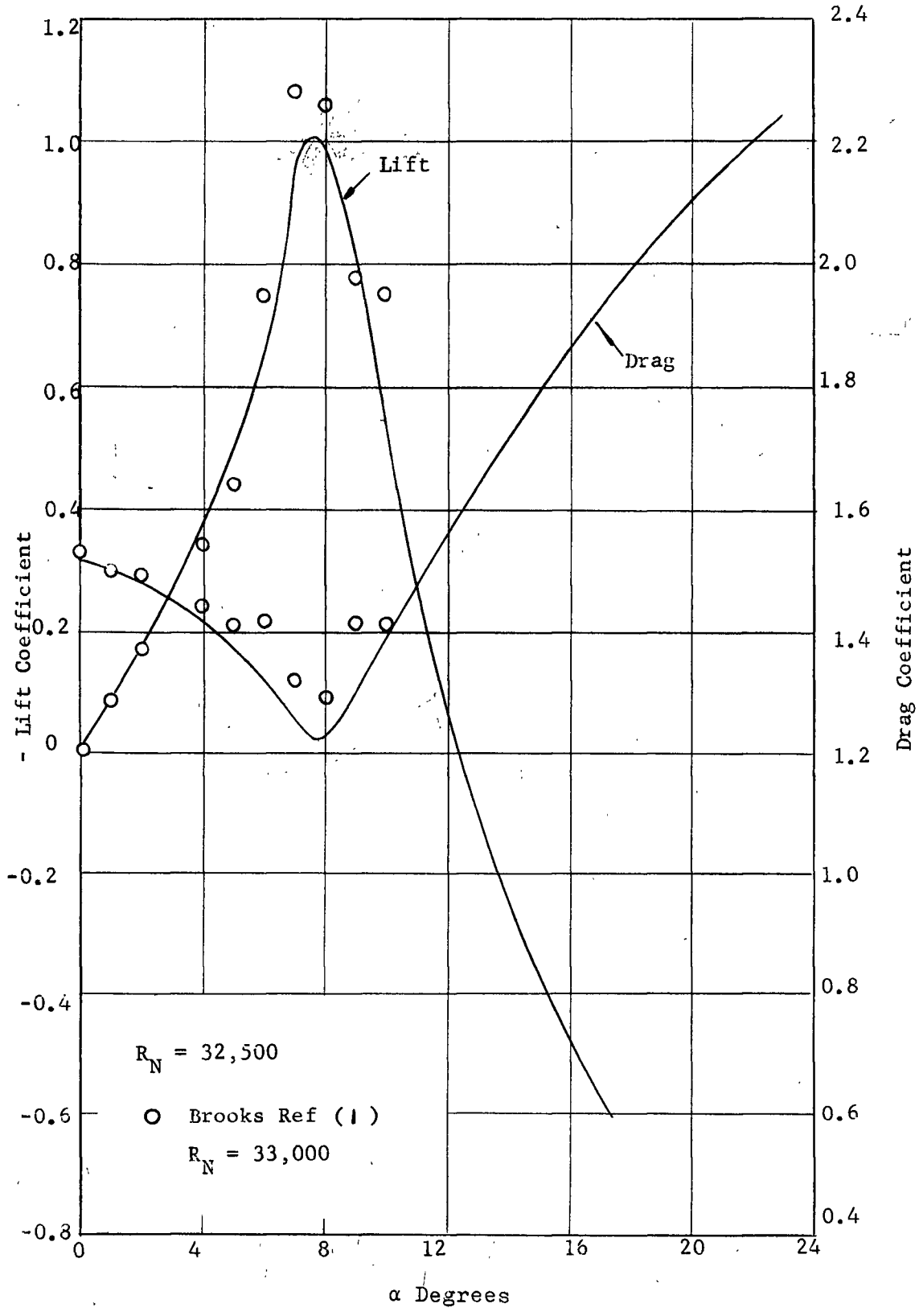

Fig. (15) Sectional Lift and Drag Coefficient for 2:1 Rectangle

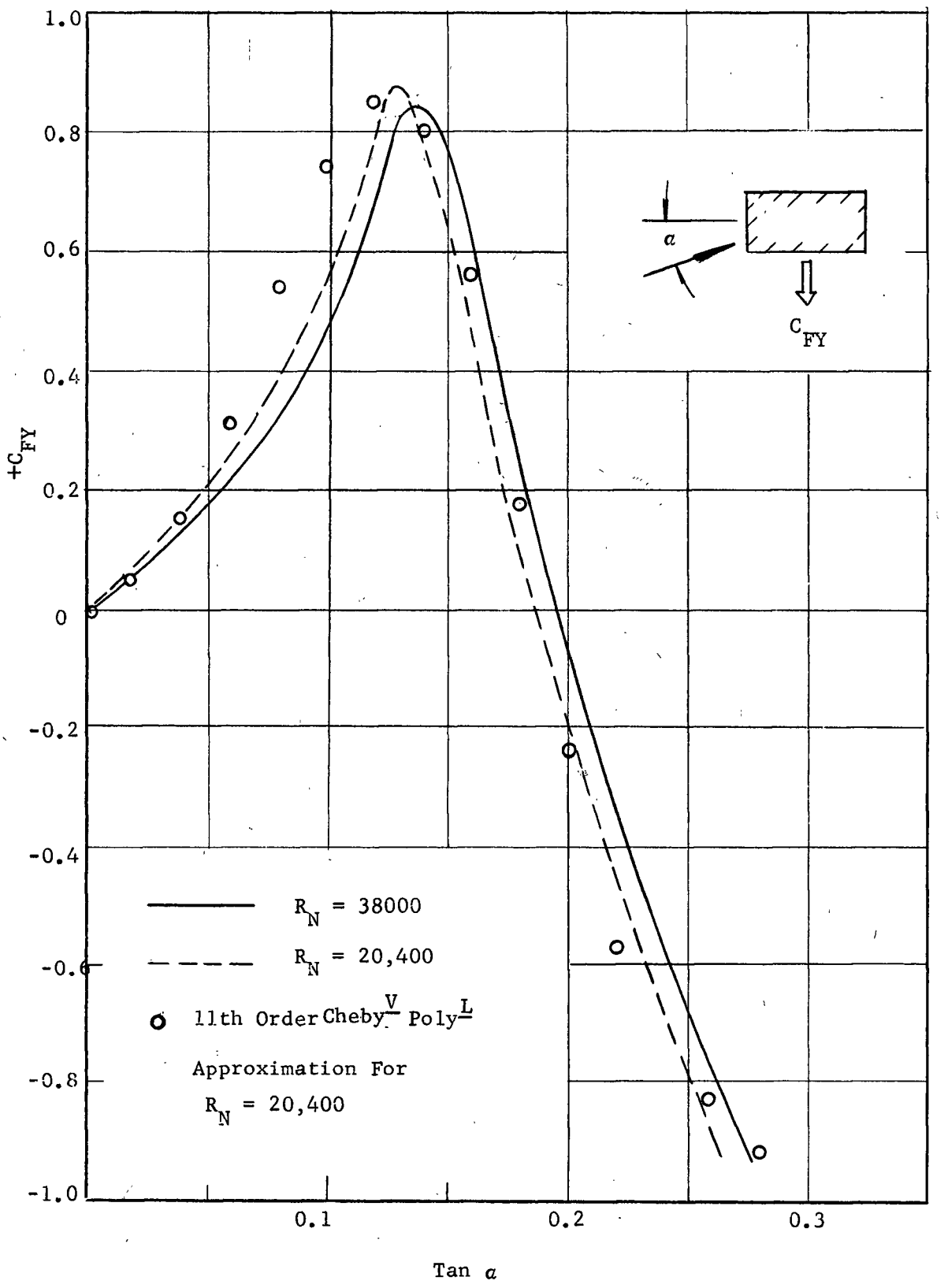

Fig. (16) C_{FY} vs Tan α for 2:1 Rectangle

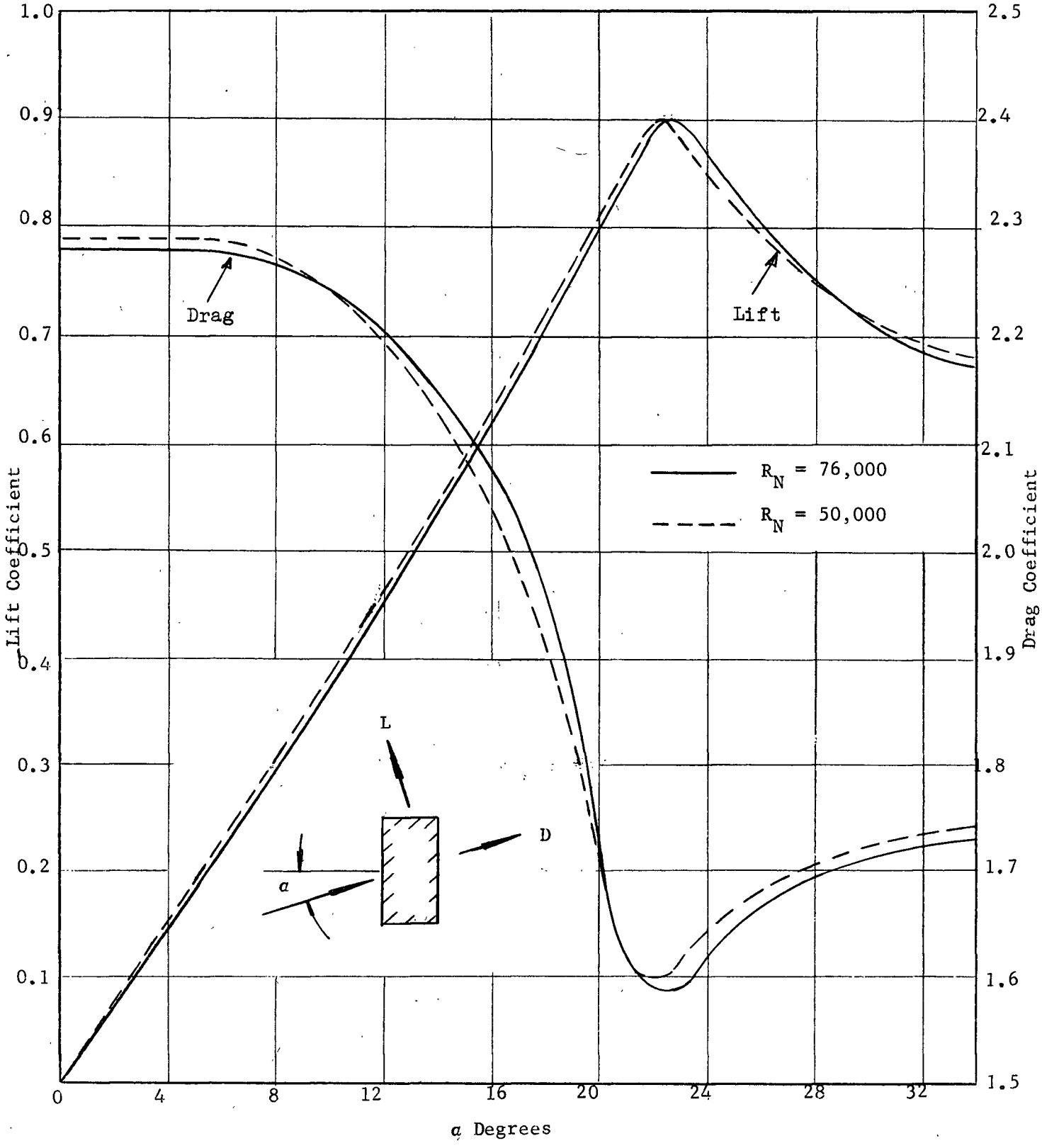

Fig. (17) Sectional Lift and Drag Coefficient for 1/2:1 Rectangle

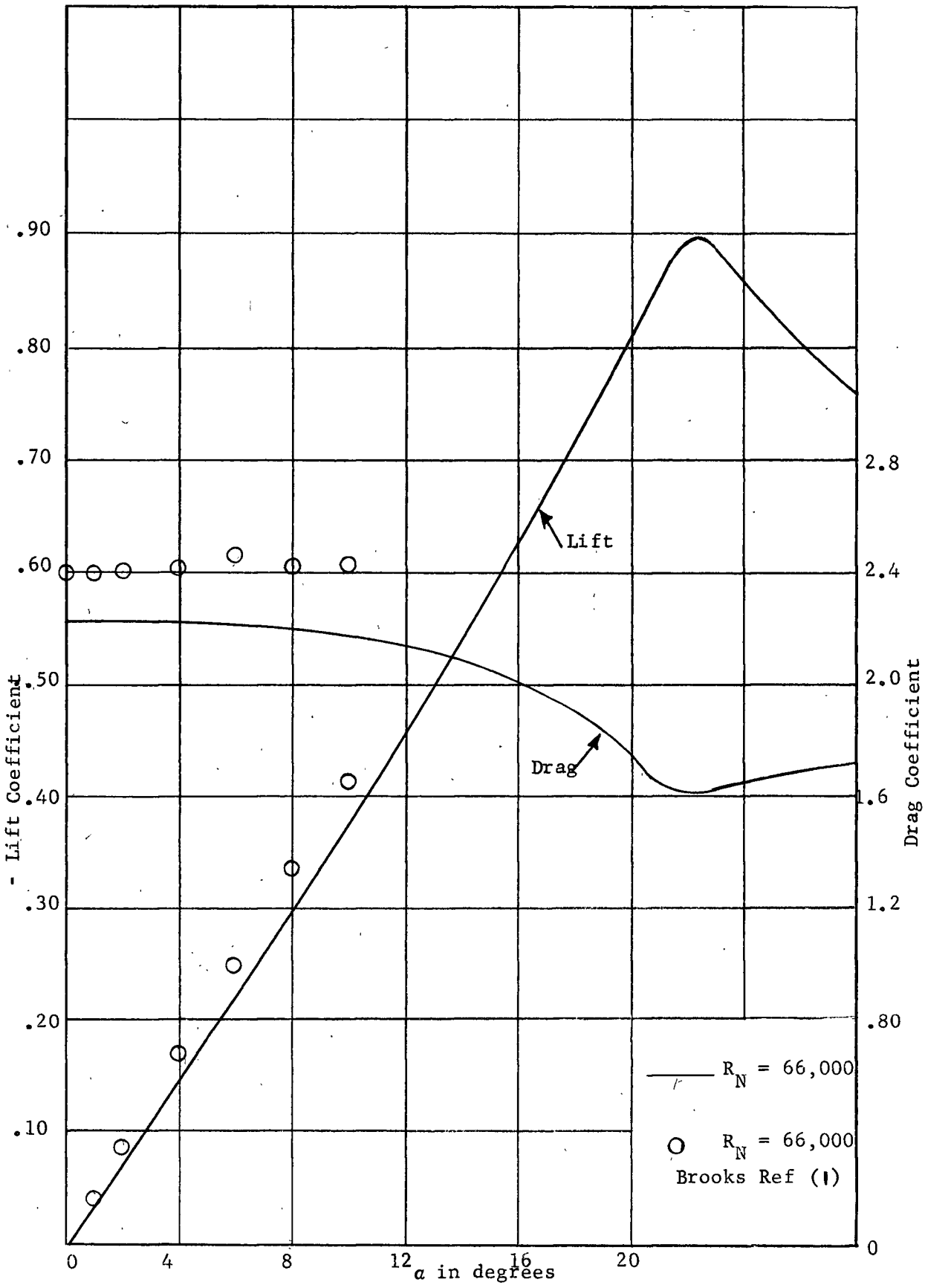

Fig. (18). Sectional Lift and Drag Coefficient for 1/2:1 Section

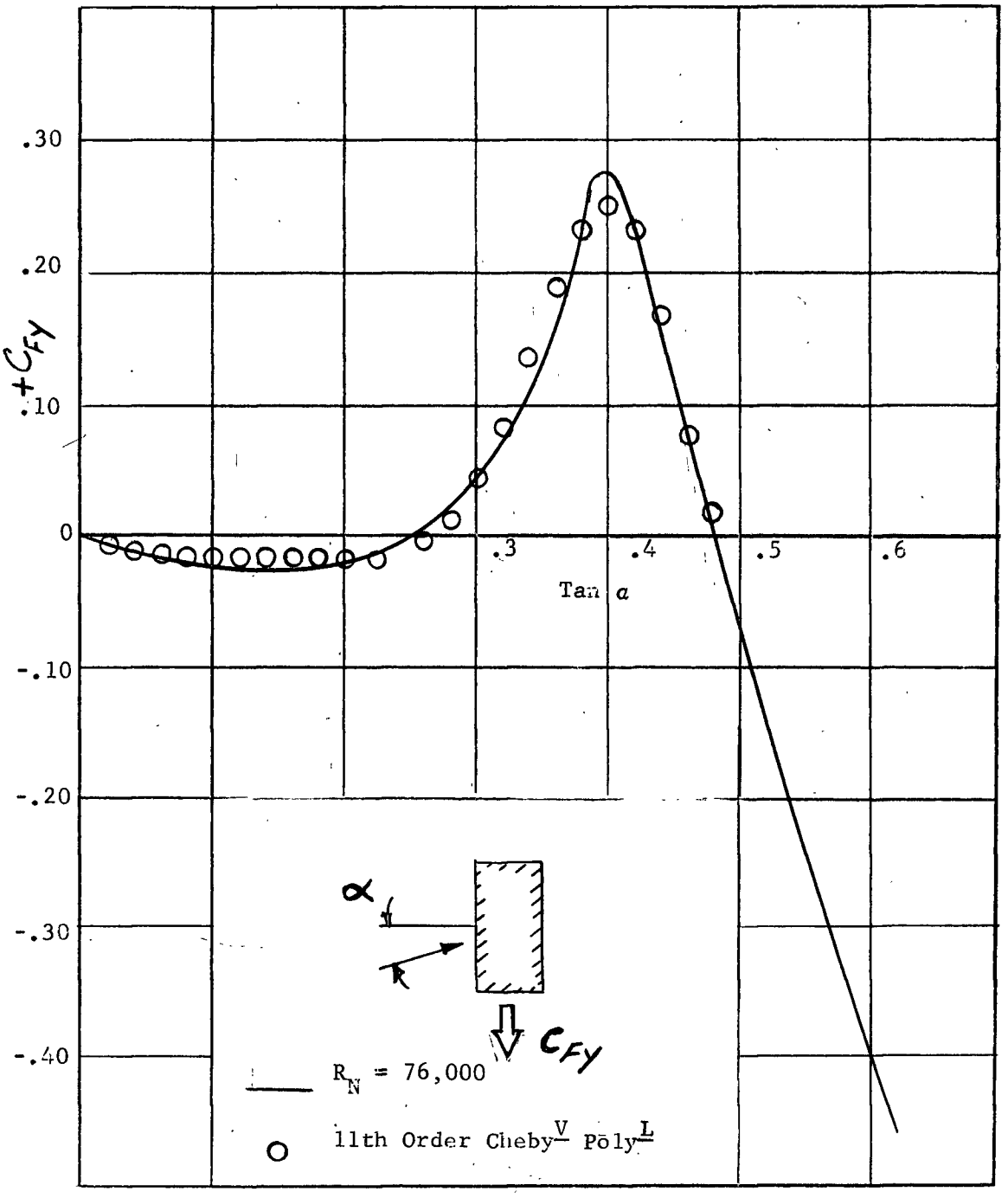

Fig. (19) C_{Fy} vs Tan α for 1/2:1 Rectangle

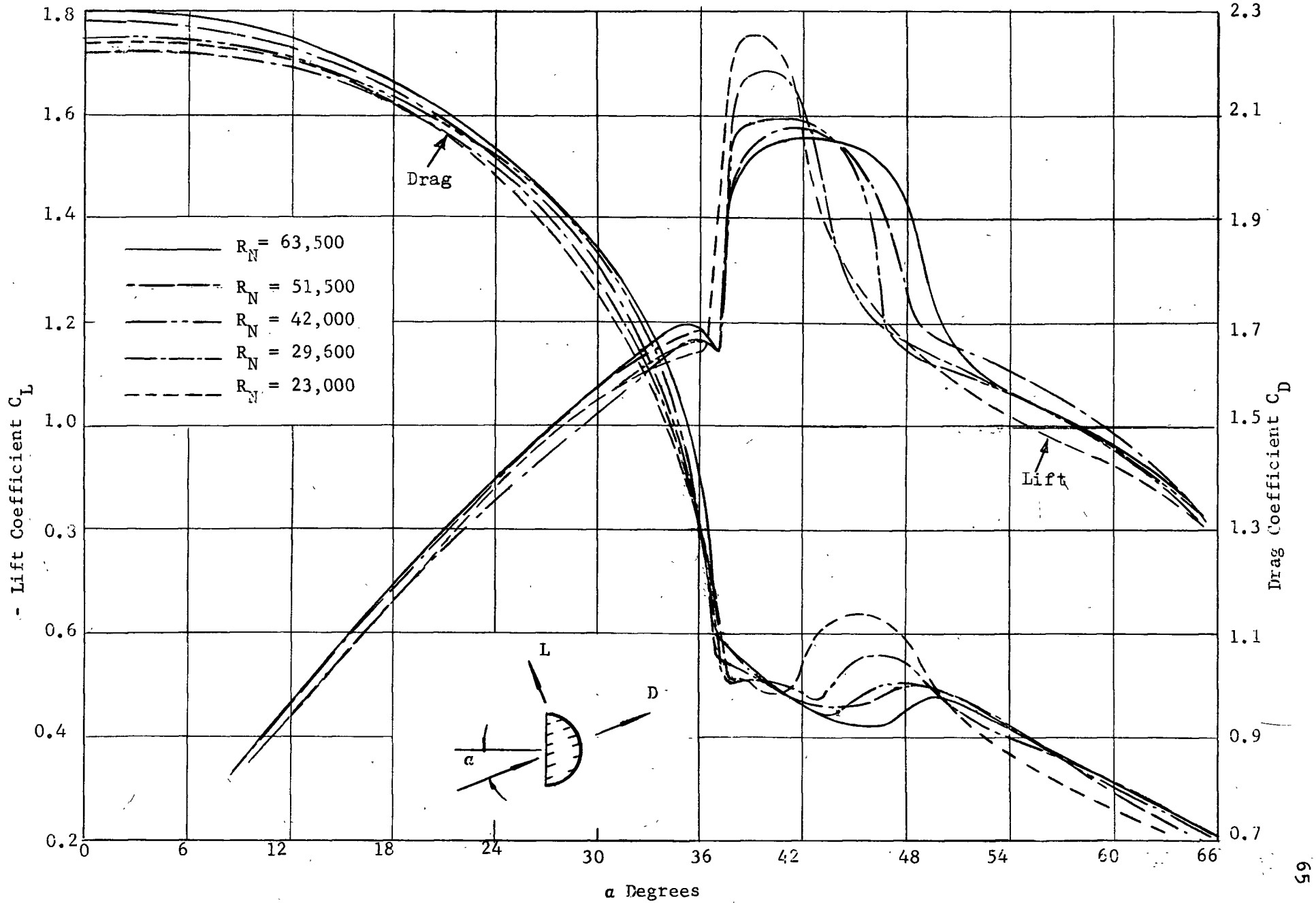

Fig. (20) Lift and Drag Coefficients for 'D' Section

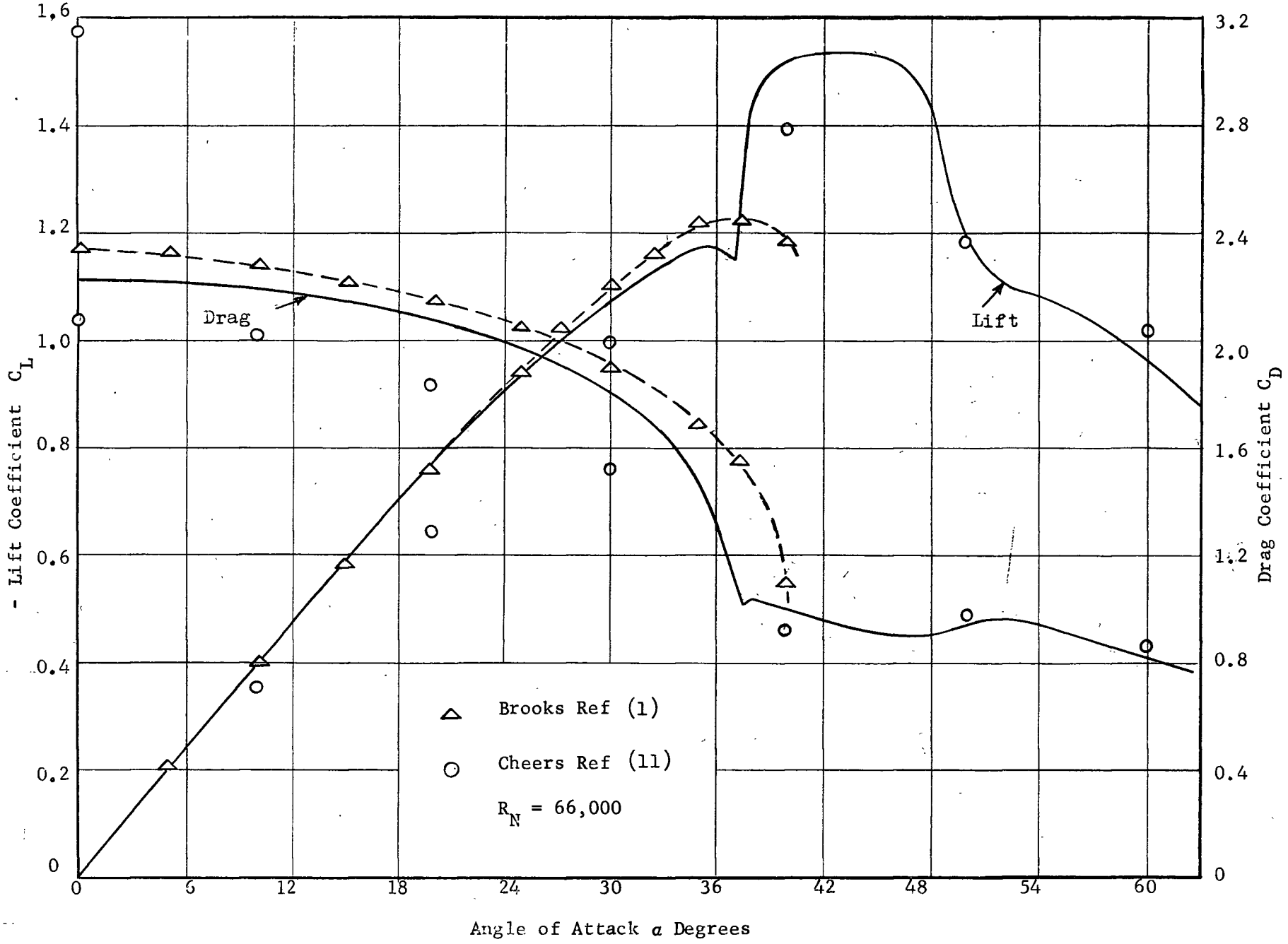

Fig. (21) Lift and Drag Coefficient for the 'D' Section

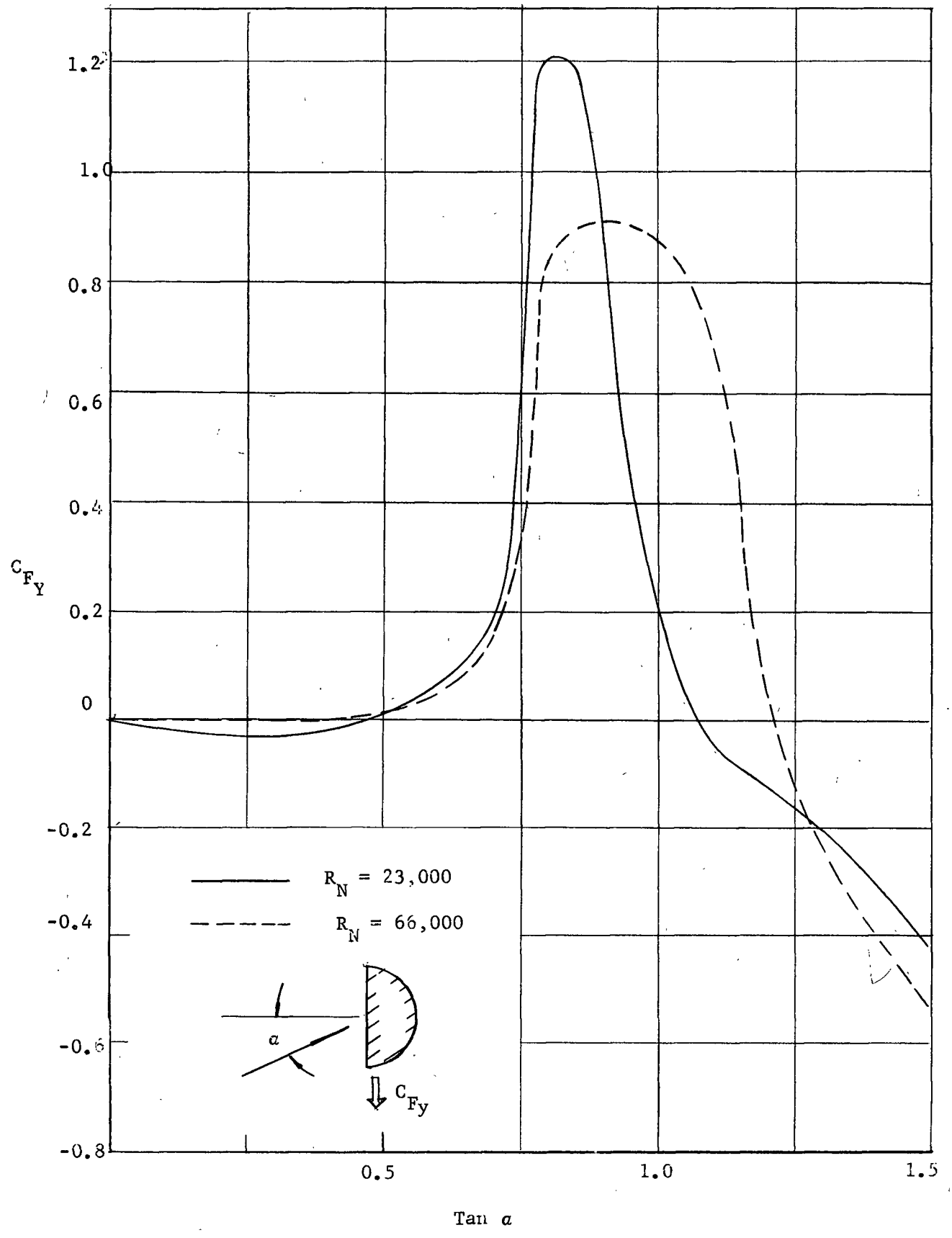

Fig. (22) C_{F_y} vs Tan α for D - Section

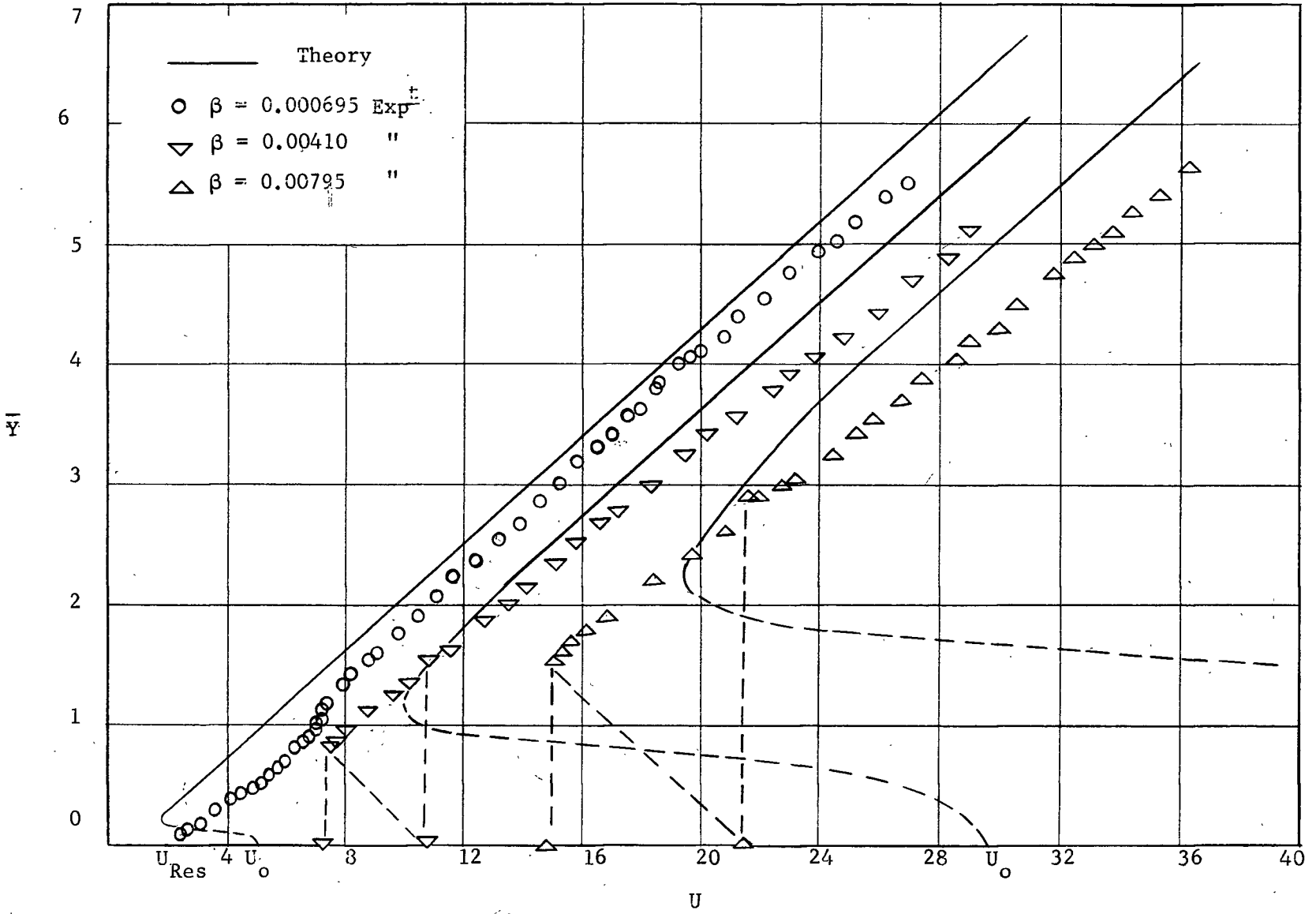

Fig. (23) Dimensionless Steady-State Plunge Amplitude vs Dimensionless Wind Velocity for A.R.2 Aluminum Model

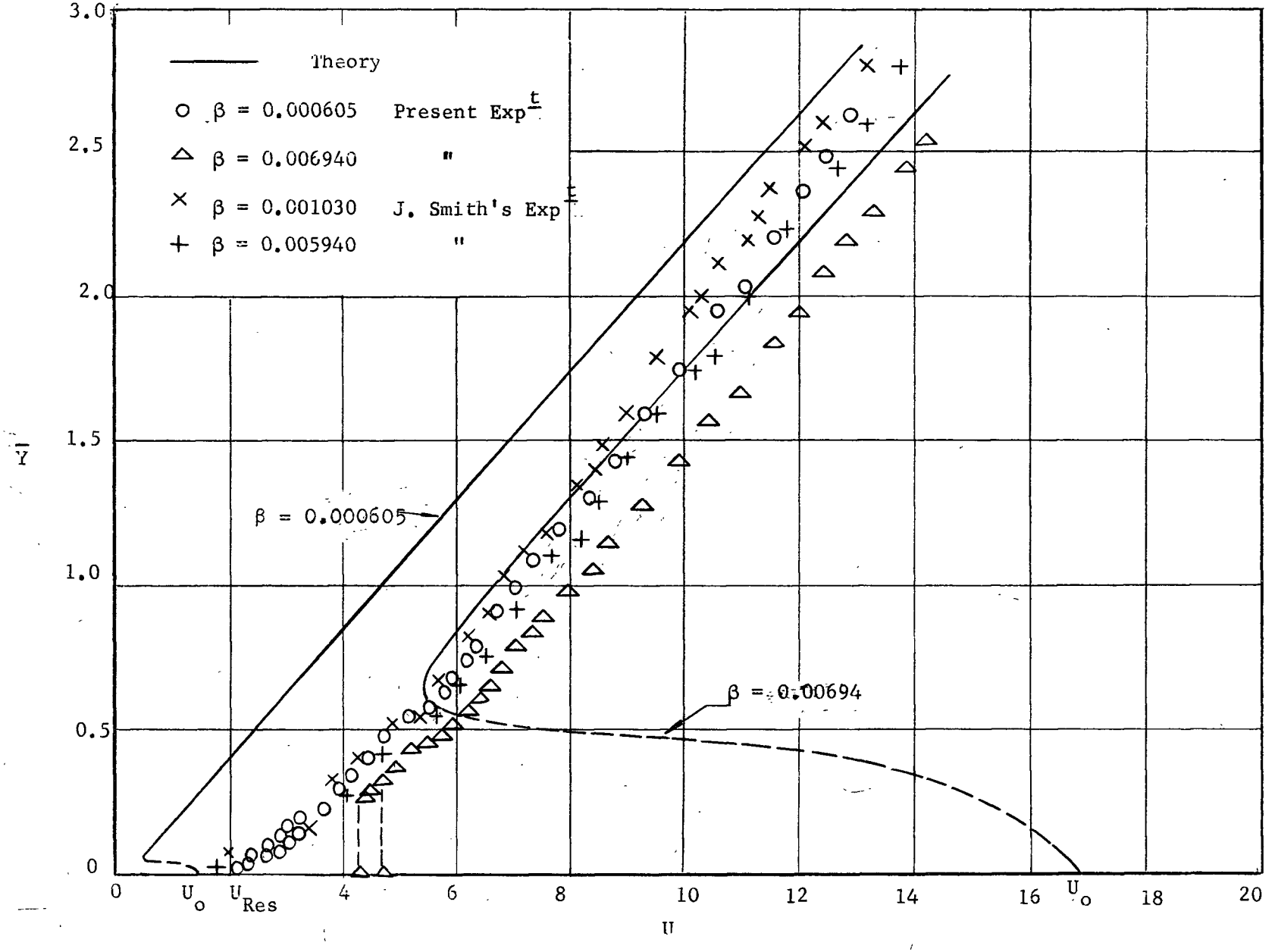

Fig. (24) Dimensionless Steady-State Plunge Amplitude vs Dimensionless Wind Velocity for A.R.2 Wooden Model

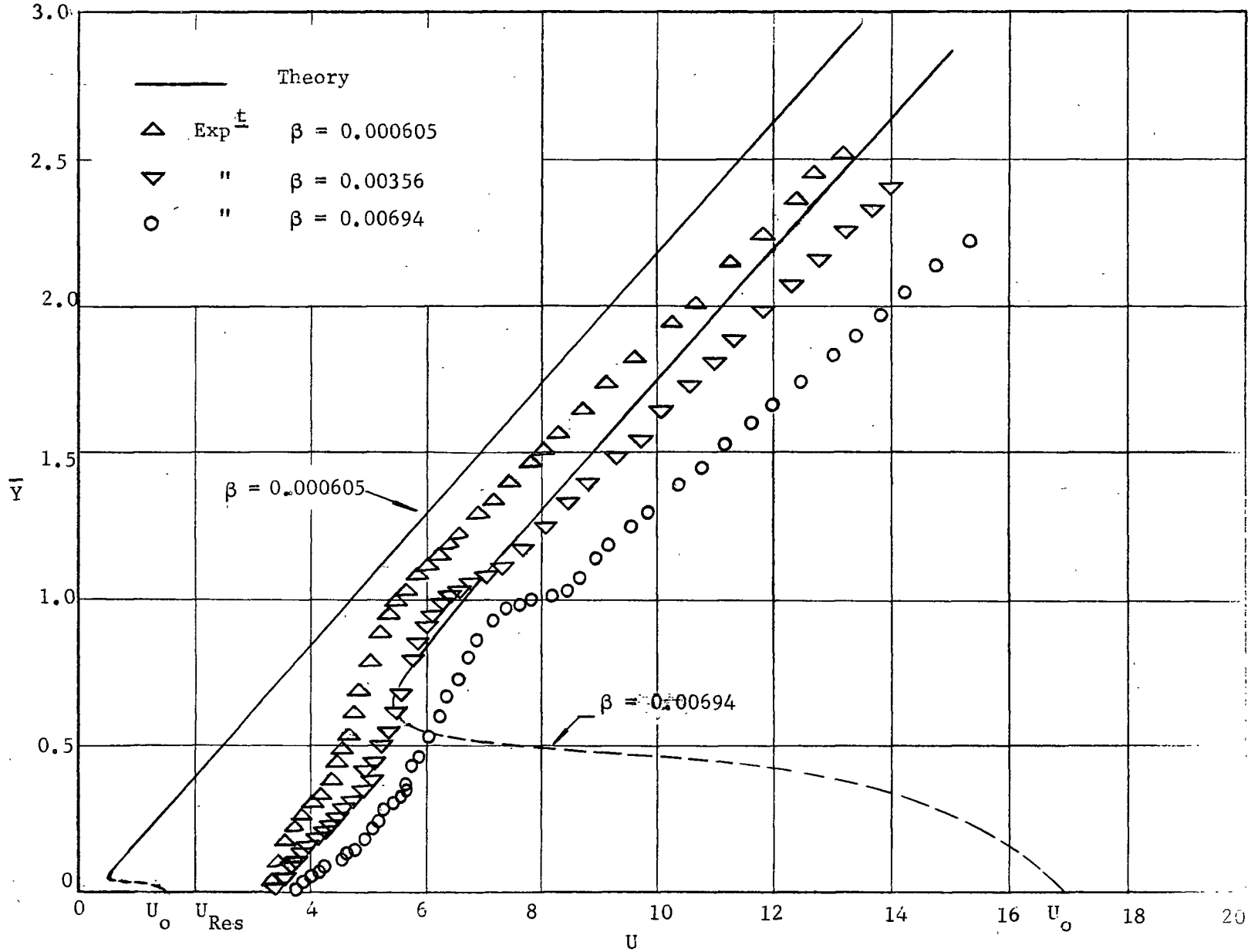

Fig (25) Dimensionless Steady-State Plunge Amplitude vs Dimensionless Wind Velocity For A.R.2 Wooden Model With 10" Splitter Plate

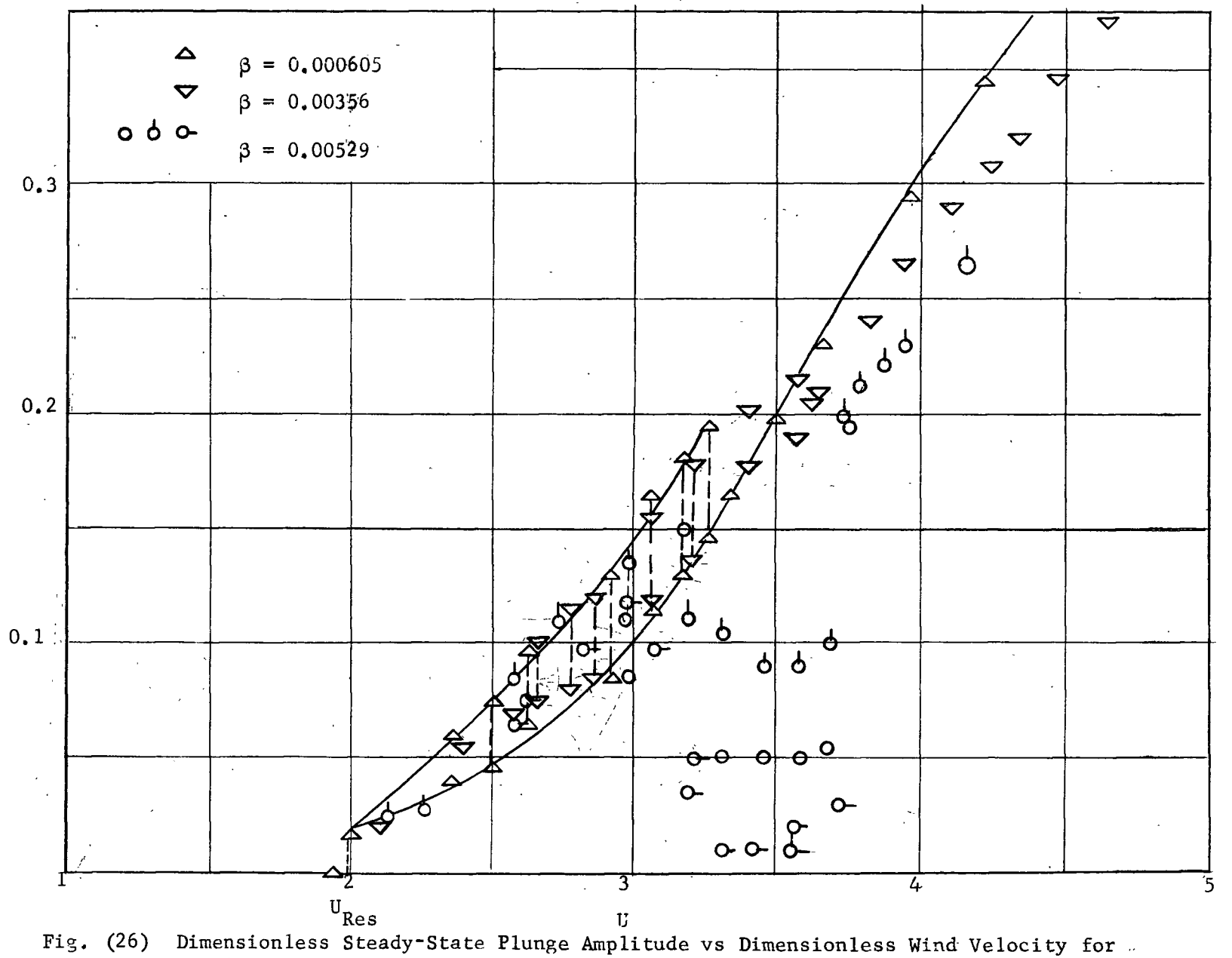

Fig. (26) Dimensionless Steady-State Plunge Amplitude vs Dimensionless Wind Velocity for A.R.2 Wooden Model

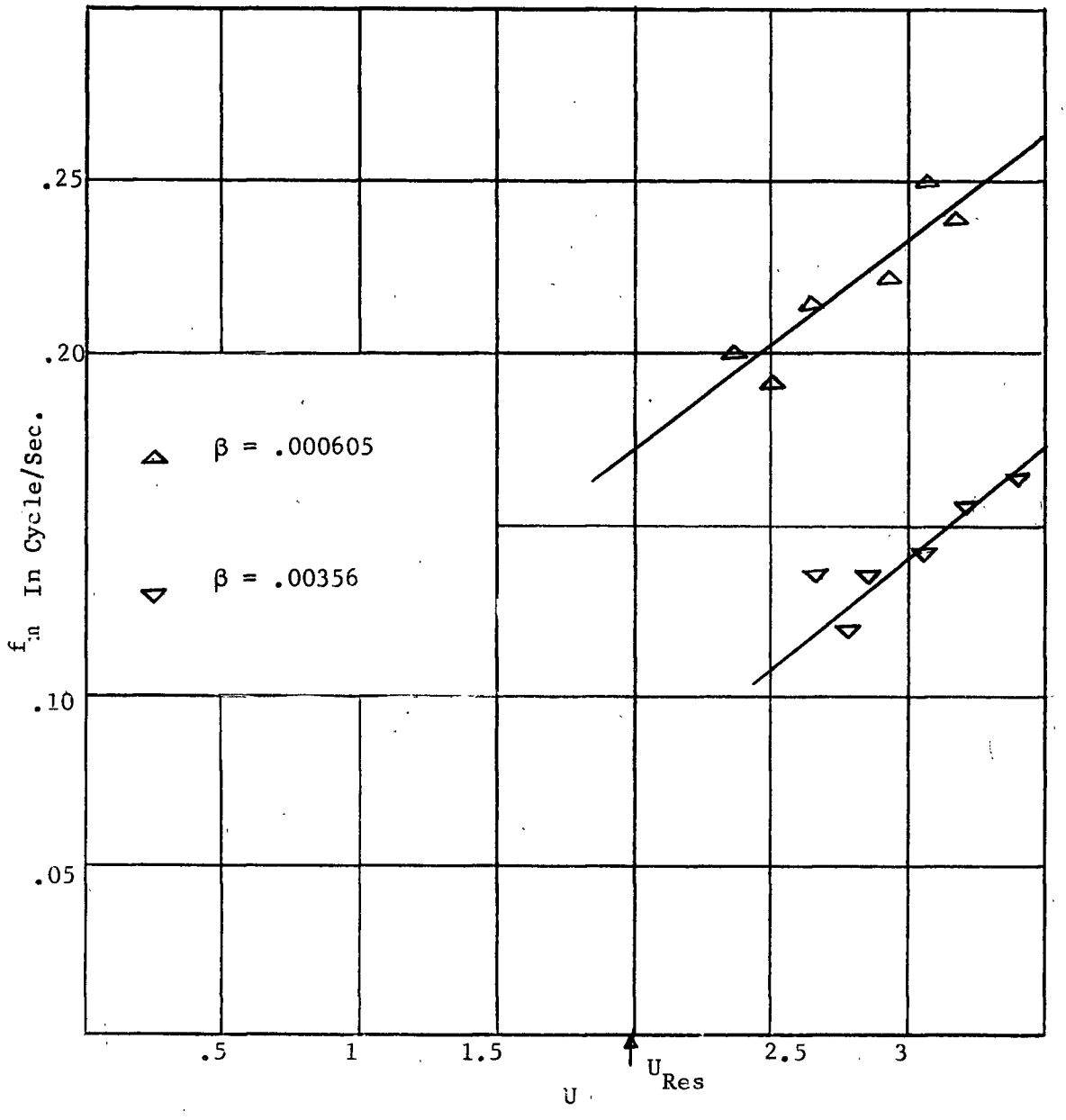

Fig. (27) Dimensionless Wind Velocity vs Modulation Frequency for A.R.2 Wooden Model

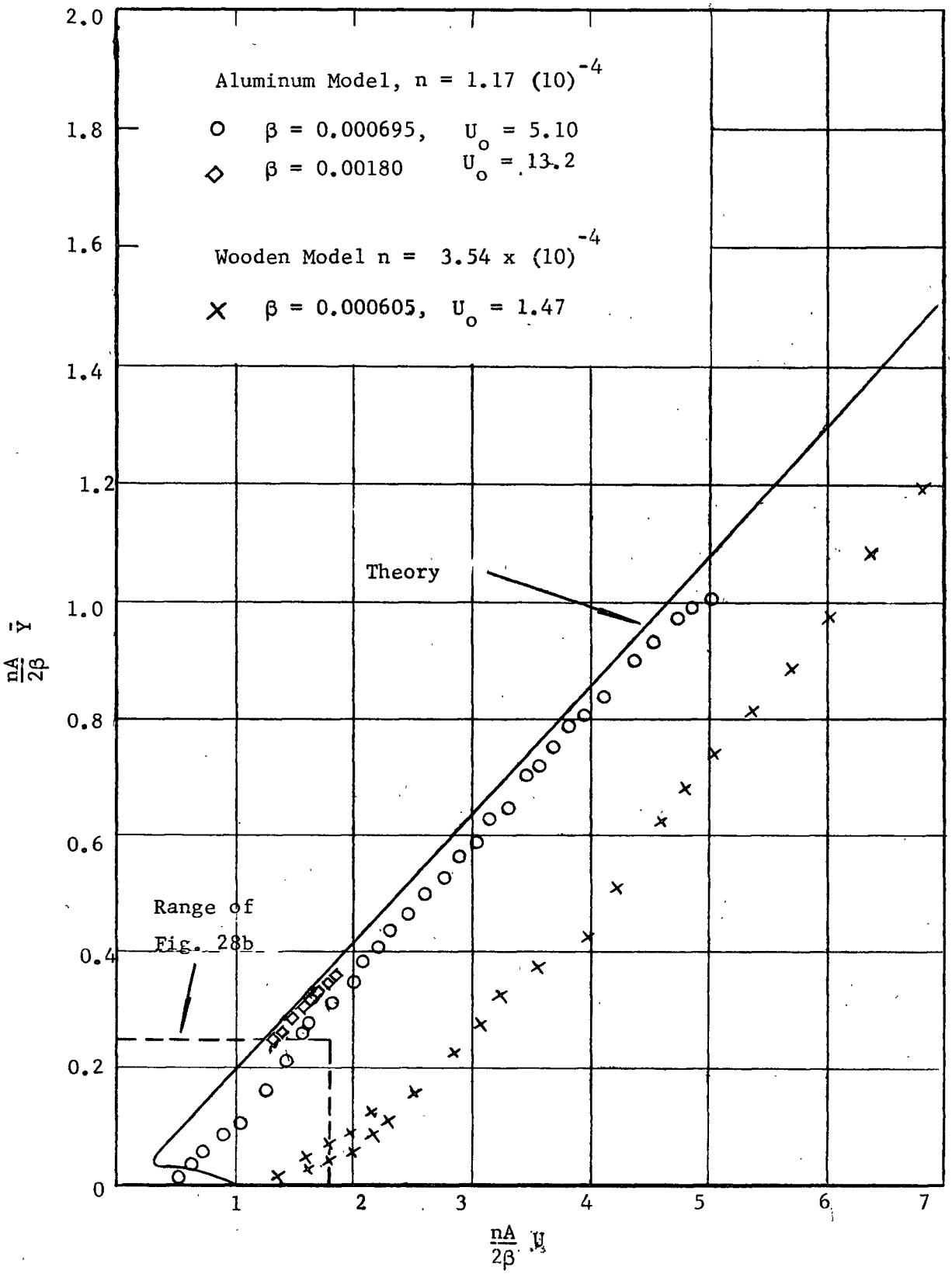

Fig. (28a) Reduced Amplitude vs Wind Speed for 2:1 Rectangle

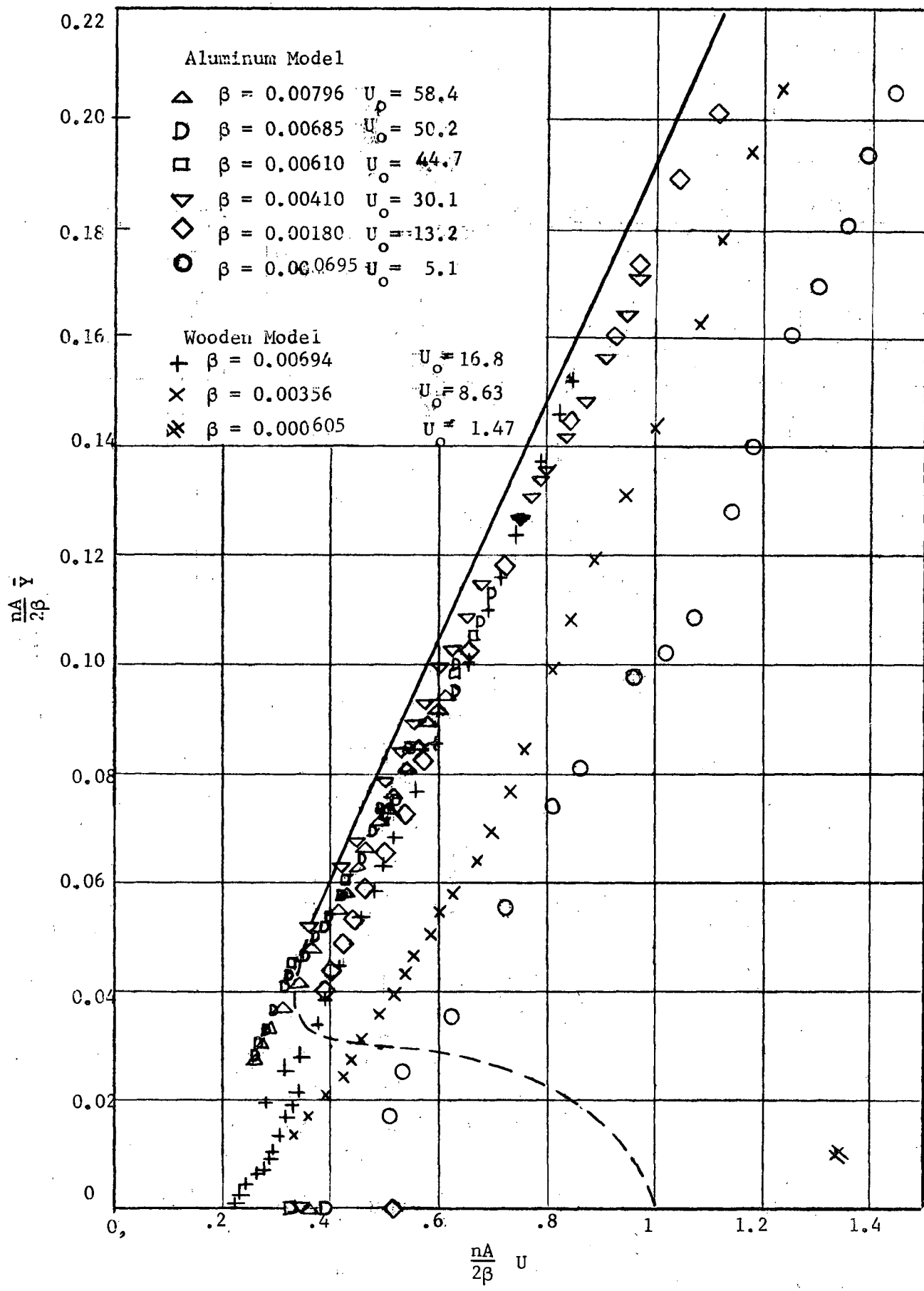
Aluminum Model
β = 0.00796 U_o = 58.4
β = 0.00685 U_o = 50.2
β = 0.00610 U_o = 44.7
β = 0.00410 U_o = 30.1
β = 0.00180 U_o = 13.2
β = 0.000695 U_o = 5.1
Wooden Model
β = 0.00694 U_o = 16.8
β = 0.00356 U_o = 8.63
β = 0.000605 U_o = 1.47
nA/2β Ȳ
nA/2β U
0.22
0.20
0.18
0.16
0.14
0.12
0.10
0.08
0.06
0.04
0.02
0
0
.2
.4
.6
.8
1
1.2
1.4

Fig. (28b)

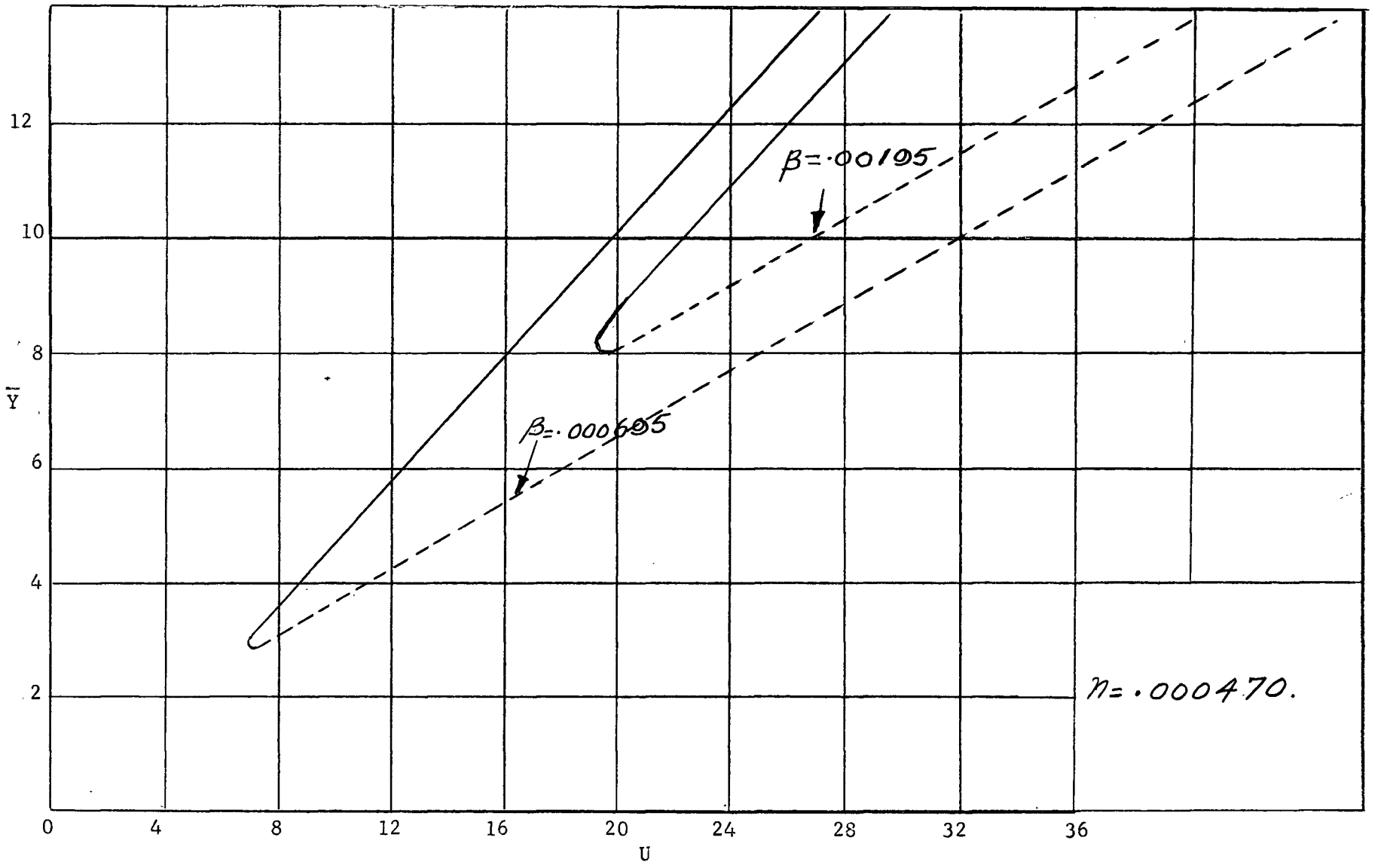

Fig. (29) Theoretical Amplitude-Velocity Curve for A.R.1/2 Aluminum Model

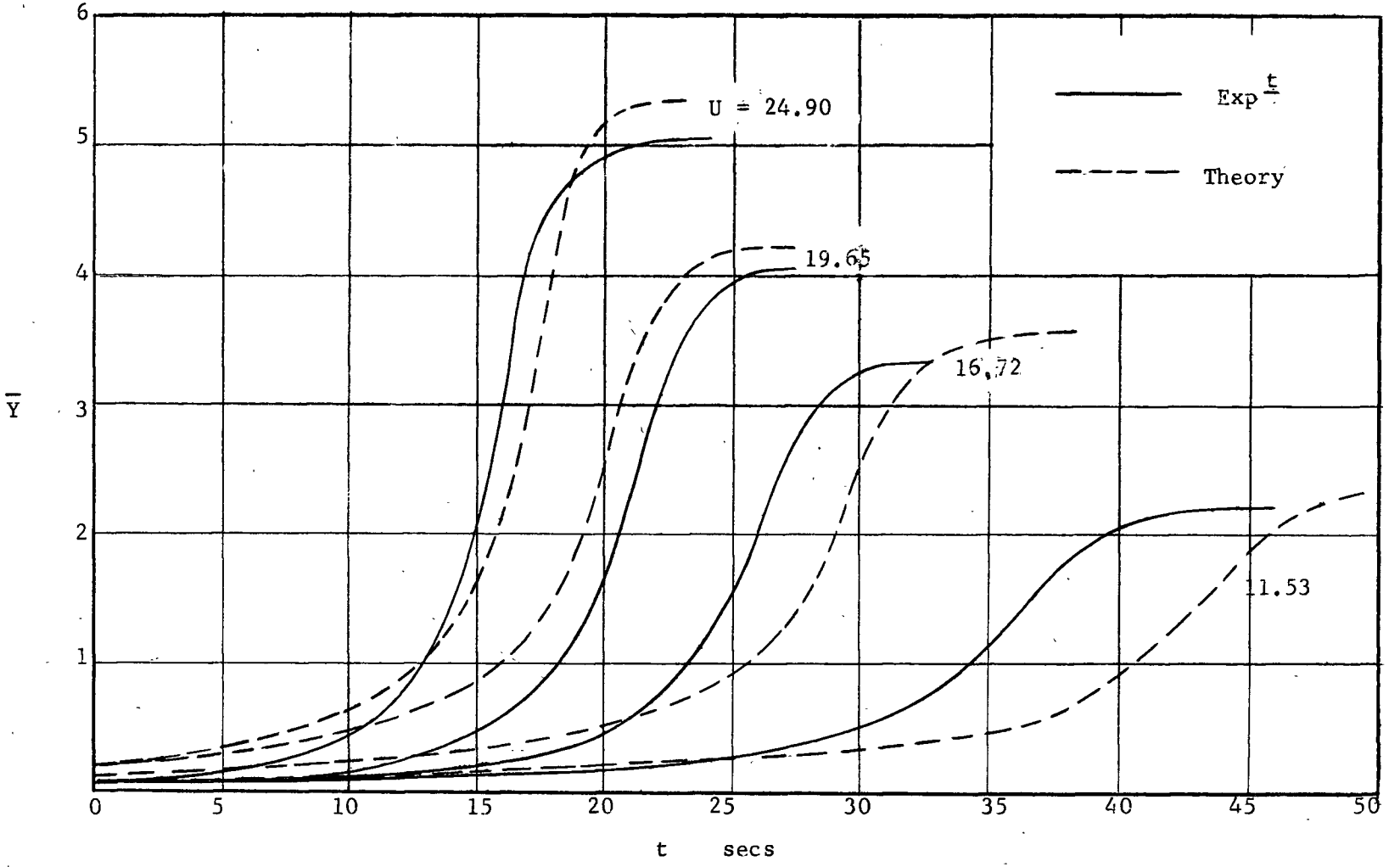

Fig. (30) Time Amplitude Curves for A.R.2 Aluminum Model

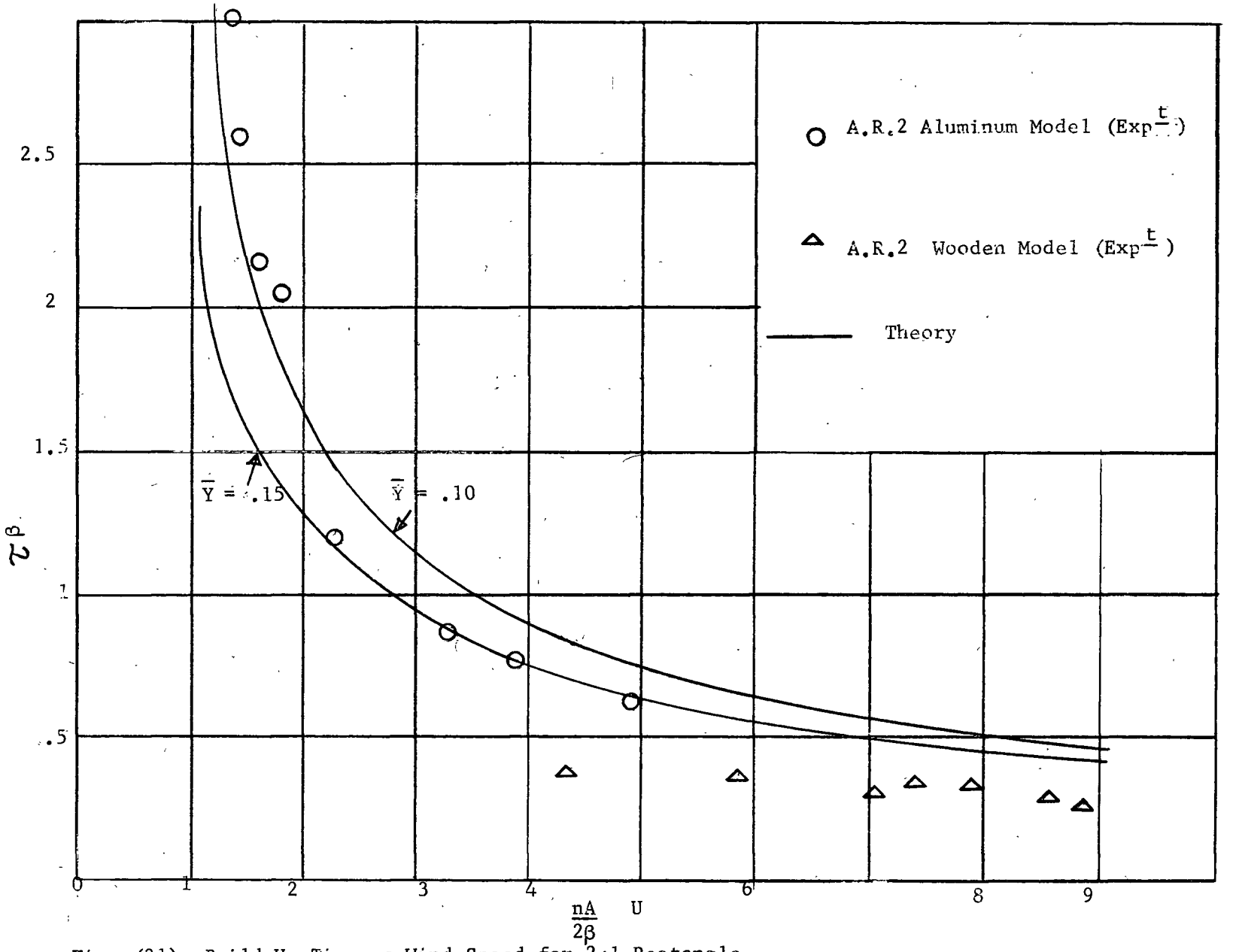

Fig. (31) Build-Up Time vs Wind Speed for 2:1 Rectangle

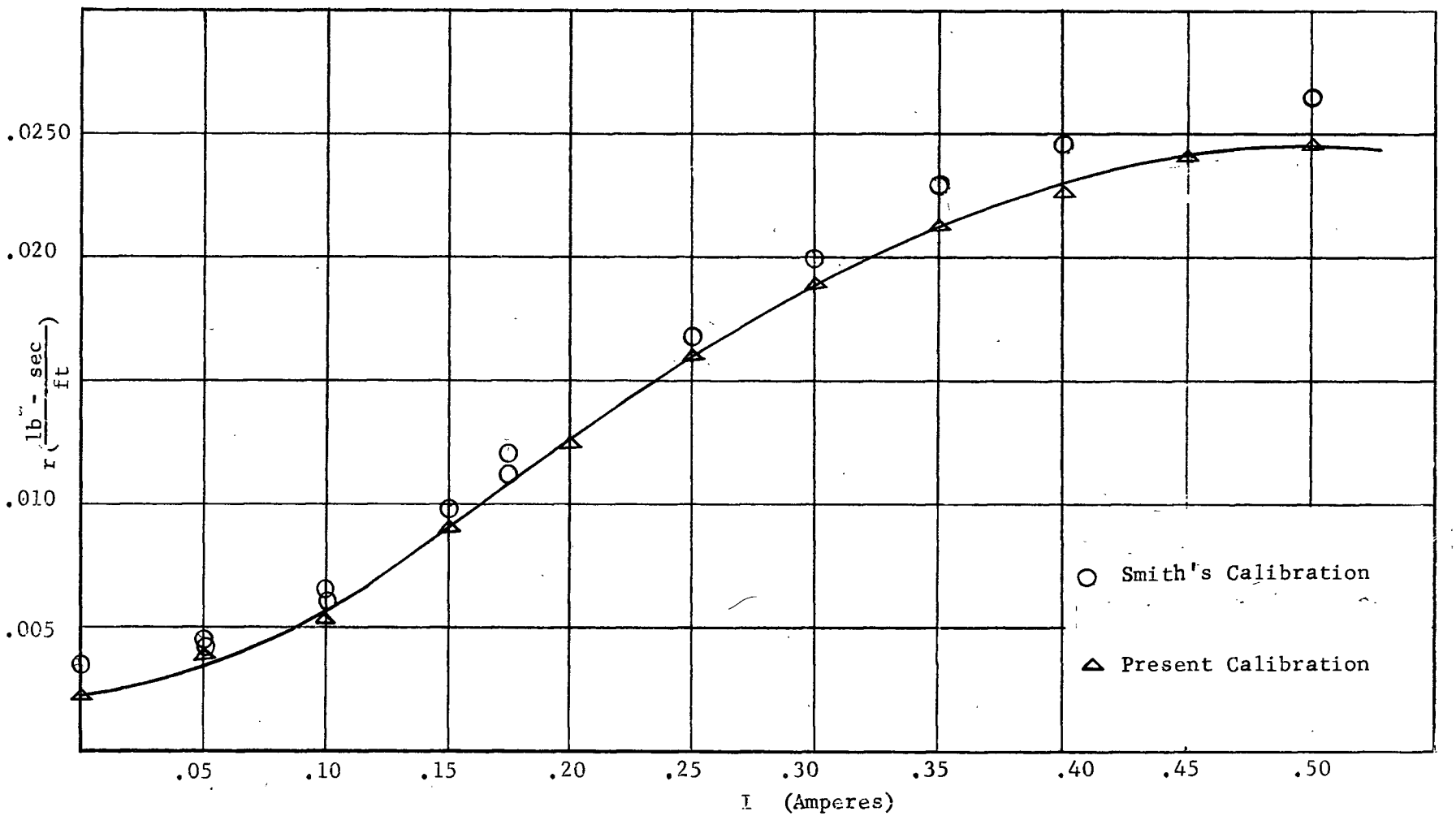

Fig. (32) Damping Calibration

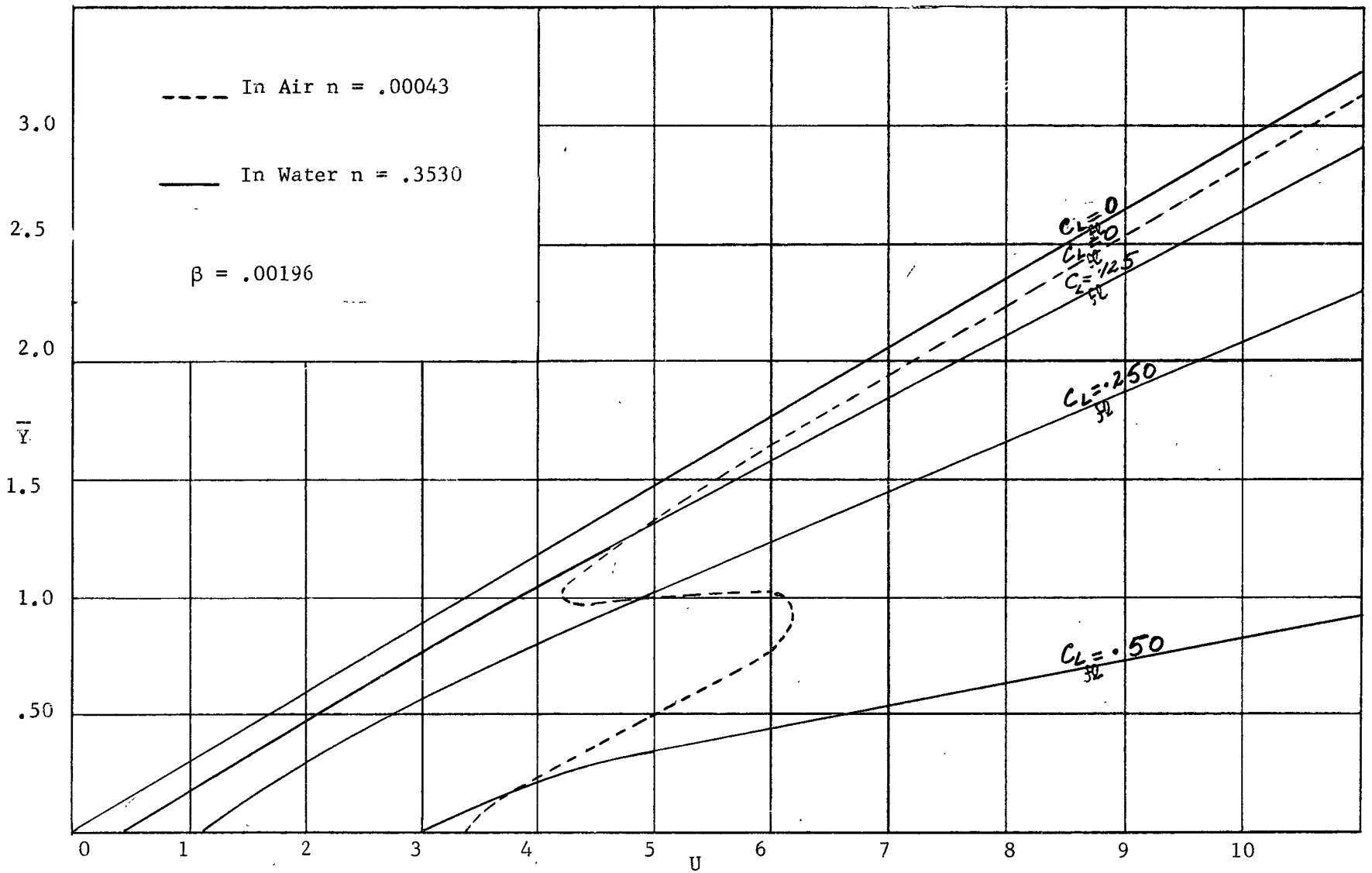

Fig. (33) Theoretical Curve of Amplitude vs Wind Velocity for a Square Prism in Air and Water for Various Lift Coefficients (Fluctuating).

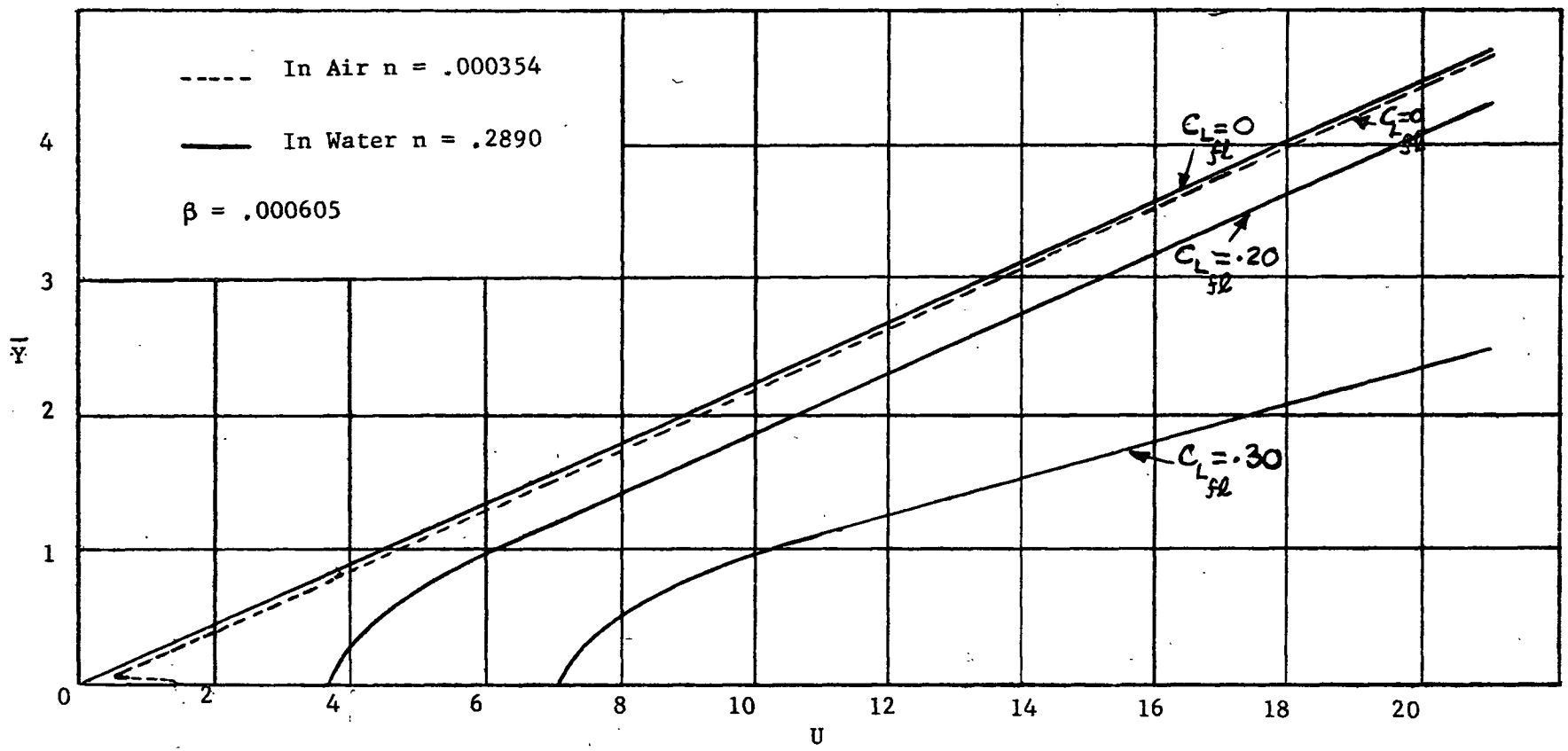

Fig. (34) Theoretical Curves of Amplitude vs Wind Velocity for the A.R.2 Wooden Model In Air and Water for Different Lift Coefficients (Fluctuating).